https://doi.org/10.5194/gmd-2020-144
Preprint. Discussion started: 7 July 2020

Geoscientific Model Development Discussions

GTS v1.0: A Macrophysics Scheme for Climate Models Based on a Probability Density Function

Chein-Jung Shiu[1,*], Yi-Chi Wang[1], Huang-Hsiung Hsu[1], Wei-Ting Chen[2], Hua-Lu Pan[3], Ruiyu Sun[4], Yi-Hsuan Chen[5], and Cheng-An Chen[1]

1 Research Center for Environmental Changes, Academia Sinica, Taiwan
2 Department of Atmospheric Sciences, National Taiwan University, Taiwan
3 Retired Senior Scientist, National Centers for Environmental Prediction, NOAA, USA
4 National Centers for Environmental Prediction, NOAA, USA
5 Department of Climate and Space Sciences and Engineering, University of Michigan, USA

Correspondence: Chein-Jung Shiu (email: cjshiu@rcec.sinica.edu.tw)

https://doi.org/10.5194/gmd-2020-144
Preprint. Discussion started: 7 July 2020

Geoscientific Model Development Discussions

Short title: Macrophysics for Climate Models

Key points:

1) A cloud macrophysics scheme utilizing grid-mean hydrometeor information is developed and evaluated for climate models.

2) The GFS-TaiESM-Sundqvist (GTS) scheme can simulate variations of cloud fraction associated with relative humidity (RH) in a more consistent way than the default scheme of CAM5.3.

3) Through a better cloud–RH relationship, the GTS scheme helps to better represent cloud fraction, cloud radiative forcing, and thermodynamic-related climatic fields in climate simulations.

https://doi.org/10.5194/gmd-2020-144
Preprint. Discussion started: 7 July 2020

Geoscientific Model Development Discussions

Abstract

Cloud macrophysics schemes are unique parameterizations for general circulation models. We propose an approach based on a probability density function (PDF) that utilizes cloud condensates and saturation ratios to replace the assumption of critical relative humidity (RH). We test this approach, called the GFS-TaiESM-Sundqvist (GTS) scheme, using the macrophysics scheme within the Community Atmospheric Model version 5.3 (CAM5.3) framework. Via single-column model results, the new approach reveals a stronger linear relationship between the cloud fraction (CF) and RH when compared to that of the default CAM5.3 scheme. We also validate the impact of the GTS scheme on global climate simulations with satellite observations. The simulated CF is comparable to CloudSat/CALIPSO data. Comparisons of the vertical distributions of CF and cloud water content (CWC), as functions of large-scale dynamic and thermodynamic parameters, with the CloudSat/CALIPSO data suggest that the GTS scheme can closely simulate observations. This is particularly noticeable for thermodynamic parameters, such as RH, upper-tropospheric temperature, and total precipitable water, implying that our scheme can simulate variation in CF associated with RH more reliably than the default scheme. Changes in CF and CWC would affect climatic fields and large-scale circulation via cloud–radiation interactions. Both climatological means and annual cycles of many of the GTS-simulated variables are improved compared with the default scheme, particularly with respect to water vapor and RH fields. Different PDF shapes in the GTS scheme also significantly affect global simulations.

https://doi.org/10.5194/gmd-2020-144
Preprint. Discussion started: 7 July 2020

Geoscientific Model Development Discussions

1. Introduction

Global weather and climate models commonly use cloud macrophysics parameterization to calculate the sub-grid cloud fraction (CF) and/or large-scale cloud condensate, as well as cloud overlap, which is required in cloud microphysics and radiation schemes [Slingo, 1987; Sundqvist, 1988; Sundqvist *et al*., 1989; Smith, 1990; Tiedtke, 1993; Xu and Randall, 1996; Rasch and Kristjansson, 1998; Jakob and Klein, 2000; Tompkins, 2002; Zhang *et al*., 2003; Wilson *et al*., 2008a,b; Chabourea and Bechtold, 2012; Park *et al*., 2014; Park *et al*., 2016]. The largest uncertainty in climate prediction is associated with clouds and aerosols [Boucher *et al*., 2013]. The large number of cloud-related parameterizations in general circulation models (GCM) contributes to this uncertainty. In recent years, an increasing amount of research has been devoted to unifying cloud-related parameterizations, for example by incorporating the planetary boundary layer, shallow and/or deep convections, and stratiform cloud (cloud macrophysics and/or microphysics) parameterizations, to improve cloud simulations in large-scale global models [Bogenschutz *et al*., 2013; Park *et al*., 2014a, 2014b; Storer *et al*., 2015].

Some of these parameterizations use prognostic approaches to parameterize the CF [Tiedtke, 1993; Tompkins, 2002; Wilson *et al*., 2008a, b; Park *et al*., 2016] while others use diagnostic approaches [Sundqvist *et al*., 1989; Smith, 1990; Xu and Randall, 1996; Zhang *et al*., 2003; Park *et al*., 2014]. Most of the diagnostic approaches used in GCM cloud macrophysical schemes use the critical relative humidity threshold (RH_c) to calculate CF [Slingo, 1987; Sundqvist *et al*., 1989; Roeckner *et al*., 1996]. In this type of parameterization, GCMs frequently use the RH_c value as a tunable parameter [Mauritsen *et al*., 2012; Golaz *et al*., 2013; Hourdin *et al*., 2016]. There are some studies on the verification of global simulations focused on the cloud macrophysical parameterization [Hogan *et al*., 2009; Franklin *et al*., 2012; Qian *et al*., 2012; Sotiropoulou *et al*., 2015]. In addition, many model development studies show the impact of total water used in CF schemes on global simulations after modifying the RH_c and/or the probability density function (PDF) [Donner *et al*., 2011; Neale *et al*., 2013; Schmidt *et al*., 2014]. Some recent studies have attempted to constrain RH_c from regional sounding observations and/or satellite retrievals to improve regional and/or global simulations [Quaas, 2012; Molod, 2012; Lin, 2014].

While many variations of the diagnostic Sundqvist CF scheme have been proposed, most numerical weather prediction models and GCMs use the basic principle proposed by Sundqvist *et al*. [1989]: the changes in cloud condensate in a grid box are derived from the budget equation for RH. In the meantime, the amount of additional moisture from other processes is divided between the cloudy portion and the clear portion

https://doi.org/10.5194/gmd-2020-144
Preprint. Discussion started: 7 July 2020


Geoscientific Model Development Discussions

according to the proportion of clouds determined using an assumed RH_c. While changes have been made to other parts of the Sundqvist scheme, the CF-RH_c relationship still applies in most Sundqvist-based schemes. As highlighted by Thompkins [2005], the RH_c value in the Sundqvist scheme can be related to the assumption of uniform distribution for the total water in an unsaturated grid box such that the distribution width (δc) of the situation when a cloud is about to form is given by:

$$\delta c = q_s(1 - RH_c), \quad (1)$$

where q_s is the saturated mixing ratio.

We re-derived this equation by describing the change in the distribution width δ with grid-mean cloud condensates and saturation ratio using the basic assumption of uniform distribution from Sundqvist *et al*. [1989] rather than using the RH_c-derived δc, thereby eliminating unnecessary use of the RH_c while retaining the PDF assumption for the entire scheme. This modified macrophysics scheme is named the GFS-TaiESM-Sundqvist (GTS) scheme version 1.0 (GTS v1.0). It was first developed for the Global Forecast System (GFS) model at the National Centers for Environmental Protection (NCEP) and has been further improved for the Taiwan Earth System Model (TaiESM; Lee *et al*., 2020) at the Research Center for Environmental Changes (RCEC), Academia Sinica. Park *et al*. [2014] discussed a similar approach wherein a triangular PDF was used to diagnose cloud liquid water as well as the cloud liquid fraction, and suggested that the PDF width could be computed internally rather than specified, to consistently diagnose both CF and cloud liquid water as in macrophysics. These authors also mentioned that such stratus cloud macrophysics could be applied across any horizontal and vertical resolution of a GCM grid, although they did not formally implement and test this idea using their scheme. Building upon their ideas, we implemented and tested this assumption with a triangular PDF in the GTS scheme.

In summary, this GTS scheme adopts Sundqvist's assumption regarding the partition of cloudy and clear regions within a model grid box but uses a variable PDF width once clouds are formed. It introduces a self-consistent diagnostic calculation of CF. Owing to their use of an internally computed PDF width, GTS schemes are expected to be able to better represent the relative variation of CF with RH in GCM grids.

A variety of assumptions regarding PDF shape can be adopted in diagnostic approaches [Sommeria and Deardorff, 1977; Bougeault, 1982; Smith, 1990; Tompkins, 2002]. Some studies have investigated representing cloud condensate and water vapor in a more statistically accurate way by using more complex types of PDF to represent parameters such as total water, CF, and updraft vertical velocity [Larson, 2002; Golaz *et al*., 2002; Firl, 2013; Bogenschutz *et al*., 2012; Bogenschutz and Krueger, 2013; Firl and Randall, 2015]. In this study, we apply and investigate two simple and commonly used PDF shapes—uniform and triangular—in our parameterization of the GTS

https://doi.org/10.5194/gmd-2020-144
Preprint. Discussion started: 7 July 2020


Geoscientific Model Development Discussions

macrophysics scheme. Other complex types of PDF assumptions can also be used if analytical solutions regarding the width of the PDF can be derived.

Most of the studies mentioned above estimate the CF via cloud liquid or total cloud water. Earlier versions of GCMs used a Slingo-type approach to resolve the cloud ice fraction [Slingo, 1987; Tompkins *et al*., 2007; Park *et al*., 2014]. On the other hand, the current generation of global models participating in the Coupled Model Intercomparison Project Phase 6 (CMIP6) have alternative approaches for the handling of CFs associated with ice clouds. In the GTS scheme, the approach to cloud liquid-water fraction parameterization is extended to the cloud ice fraction as well, wherein the saturation-mixing ratio (q_s) with respect to water is replaced by q_s with respect to ice. This provides a consistent treatment for the cloud liquid and cloud ice fractions. Many studies have argued that the assumption of rapid adjustment between water vapor and cloud liquid water applied in GCM CF schemes cannot be applied to ice clouds [Tompkins *et al*., 2007; Salzmann *et al*., 2010; Chosson *et al*., 2014]. In addition, it would be difficult to represent the CF of mixed-phase clouds using such an assumption [McCoy *et al*., 2016]. Applying a diagnostic approach to the cloud ice fraction similar to that used for the cloud liquid fraction is indeed challenging and may result in a high level of uncertainty. To investigate this issue, we also conduct a series of sensitivity tests related to the super-saturation ratio assumption, which is applied when calculating the cloud ice fraction in the GTS scheme.

2. Descriptions of scheme, model, and simulation setup

2.1 Scheme descriptions

Figure 1 illustrates the PDF-based scheme with a uniform PDF and a triangular PDF of total water substance q_t. By assuming that the clear region is free of condensates and that the cloudy region is fully saturated, the cloudy region (b) becomes the area where q_t is larger than the saturation value q_s (shaded area). The PDF-based scheme automatically retains consistency between CF and condensates because it is derived from the same PDF. Here, we used the uniform PDF to demonstrate the relationship between RH_c and the width of the PDF. Using a derivation extended from Thompkins [2005]:

$$b = \frac{1}{2\delta}(q_t + \delta - q_s). \quad (2)$$

It is evident that, with the uniform PDF:

$$\delta_c = q_s(1 - RH_c). \quad (3)$$

Therefore, $RH_c = 1 - \frac{\delta_c}{q_s}$. Thus, if the width δ of the uniform PDF is determined, then

https://doi.org/10.5194/gmd-2020-144
Preprint. Discussion started: 7 July 2020

Geoscientific Model Development Discussions

RH_c can be determined accordingly. This relation reveals that the RH_c assumption of the RH-based scheme actually assumes the width of the uniform PDF to be δc from the PDF-based scheme. As noticed by Thompkins [2005], the RH_c used by Sundqvist *et al.* [1989] for cloud generation can be linked to the statistical cloud scheme with a uniform distribution. Building upon this finding, we eliminated the assumption of RH_c by determining the $P(q_t)$ with information about q_V and q_L provided by the base model.

In addition to the application of a PDF-based approach for liquid CF parameterization, the GTS scheme also uses the same concept for parameterizing the ice CF (b_i) as follows:

$$b_i = \frac{1}{2\delta}(\overline{q_I} + \overline{q_V} + \delta - sup * q_{si}), \tag{4}$$

where $\overline{q_I}$, $\overline{q_V}$, and q_{si} denote the grid-mean cloud-ice mixing ratio, water-vapor mixing ratio, and saturation mixing ratio over ice, respectively. In equation (4), q_{si} is multiplied by a supersaturation factor (*sup*) to account for the situation in which rapid saturation adjustment is not reached for cloud ice. In the present version of the GTS scheme, *sup* is temporarily assumed to be 1.0. Sensitivity tests regarding *sup* will be discussed in Section 5.6.

A more complex PDF can be used for $P(q_t)$ instead of the uniform distribution in our derivation. For example, the Community Atmospheric Model version 5.3 (CAM5.3) macrophysics model adopts a triangular PDF instead of a uniform PDF to represent the sub-grid distribution of the total water substance [Park *et al.*, 2014]. Mathematically, the triangular distribution is a more accurate approximation of the Gaussian distribution than the uniform distribution and it may also be more realistic. Therefore, we followed the same procedure to diagnose the CF by forming a triangular PDF with $\overline{q_L}$, $\overline{q_V}$, and $\overline{q_s}$ provided. Moreover, by using a triangular PDF, we can obtain results that are more comparable with the CAM5.3 macrophysics scheme because the same PDF was used. By considering the PDF width, the CF (b) and liquid water content ($\overline{q_L}$) can be written as follows:

$$b = \begin{cases} \frac{1}{2}(1 - s_s)^2 \; if \; s_s > 0 \\ 1 - \frac{1}{2}(1 - s_s)^2 \; if \; s_s < 0 \end{cases} \tag{5}$$

and:

$$\frac{q_L}{\delta} = \begin{cases} \frac{1}{6} - \frac{{s_s}^2}{2} + \frac{{s_s}^3}{3} - s_s b \\ \frac{1}{6} - \frac{1}{6}(3{s_s}^2 - 2{s_s}^3) - s_s b \end{cases}, \tag{6}$$

respectively, where $s_s = \frac{q_s - \overline{q_t}}{\delta}$. From these two equations, we can derive the width of the triangular PDF and calculate the CF (b) based on q_s, q_t, and $\underline{q_L}$ instead of RH_c.

https://doi.org/10.5194/gmd-2020-144
Preprint. Discussion started: 7 July 2020


Geoscientific Model Development Discussions

Notably, the PDF width for the total water substance can only be constrained when the cloud exists. Therefore, the RH_c is still required when clouds start to form from a clear region.

In this study, GTS schemes utilizing two different PDF shape assumptions are evaluated: uniform (hereafter, U_pdf) and triangular (hereafter, T_pdf). These two PDF types are specifically formulated to evaluate the effects of the choice of PDF shape. A triangular PDF is the default shape used for cloud macrophysics by the Community Atmospheric Model version 5.3 (CAM5.3; hereafter, the Park scheme). The T_pdf of the GTS scheme is numerically similar to that of the Park scheme except for using a variable width for the triangular PDF once clouds are formed.

2.2 Model description and simulation setup

The GTS schemes described in this study were implemented into CAM5.3 in the Community Earth System Model version 1.2.2 (CESM 1.2.2), which is developed and maintained by DOE UCAR/NCAR. Physical parameterizations of CAM5.3 include deep convection, shallow convection, macrophysics, aerosol activation, stratiform microphysics, wet deposition of aerosols, radiation, a chemistry and aerosol module, moist turbulence, dry deposition of aerosols, and dynamics. References for the individual physical parameterizations can be found in the NCAR technical notes [Neale *et al.*, 2010]. The master equations are solved on a vertical hybrid pressure−sigma coordinate system (30 vertical levels) using the finite-volume dynamical core option of CAM5.3.

We conducted both the single-column tests and stand-alone global-domain simulations with CAM5.3 physics. The single-column setup provides the benefit of understanding the responses of physical schemes under environmental forcing of different regimes of interest. Here, we adopt the case of Tropical Western Pacific–International Cloud Experiment (TWP-ICE), which was supported by the ARM program of the Department of Energy and the Bureau of Meteorology of Australia from January to February 2006 over Darwin in Northern Australia. Based on the meteorological conditions, the TWP-ICE period can be divided into four shorter periods: the active monsoon period (19–25 January), the suppressed monsoon period (26 January to 2 February), the monsoon clear-sky period (3–5 February), and the monsoon break period (6–13 February, May *et al*. [2008]; Xie *et al*. [2010]). To take advantage of previous studies of cloud-resolving models and single-column models, we followed the setup of Franklin *et al*. [2012] to initiate the single-column runs starting on 19 January, 2006, and running for 25 days.

Stand-alone CAM5.3 simulations of the CESM model, forced by climatological sea surface temperature for the year 2000 (*i.e.*, CESM compset: F_2000_CAM5), are

https://doi.org/10.5194/gmd-2020-144
Preprint. Discussion started: 7 July 2020

conducted to demonstrate global results. The horizontal resolution of the CESM global runs is set at 2°. Individual global simulations are integrated for 12 years, and the output for the last 10 years is used to calculate climatological means and annual cycles in global means. Because we made changes largely with respect to CF, we also conducted corresponding simulations using the satellite-simulator approach to provide CF for a fair comparison with satellite CF products and typical CESM model output. This was done using the CFMIP Observation Simulator Package (COSP) built into CESM 1.2.2 [Kay *et al*., 2012]. In addition to the default monthly outputs, daily outputs of several selected variables are also written out for more in-depth analysis.

3. Observational datasets and offline calculations

3.1 Observational data

Cloud field comparisons are critical for modifications to our system with respect to cloud macrophysical schemes. Therefore, we use the products from CloudSat/CALIPSO to provide CF and CWC data for evaluating the modeling capabilities of the default and modified GTS cloud macrophysical schemes.

In addition to cloud observations, observational radiation fluxes from CERES-EBAF are also used to investigate whether simulations using our system will improve radiation calculations for both shortwave and longwave radiation flux, as well as their corresponding cloud radiative forcings. Precipitation data are compared with Global Precipitation Climatology Project data and several other climatic parameters, *e.g.*, air temperature, RH, precipitable water, and zonal wind, are evaluated against the reanalysis data (ERA-Interim).

We further evaluate the performance of the three macrophysics schemes by using the approach of Su *et al*. [2013], which compares CF and CWC sorted by large-scale dynamical and thermodynamic parameters. The CF products are based on the 2B-GEOPROF R04 dataset [Marchand *et al*., 2008], while the CWC data are based on the 2B-CWC-RO R04 dataset [Austin *et al*., 2009]. The methodology from Li *et al*. [2012] is used to generate gridded data. Four years of CloudSat/CALIPSO data, from 2007 to 2010, are used to carry out the statistical analyses. These data are used to obtain overall climatological means to compare to those obtained from model simulations instead of undergoing rigorous year-to-year comparisons between observations and simulations. Monthly data from ERA-Interim for the same four years are used to obtain the dynamical and thermodynamic parameters used in Su *et al*.'s approach. These parameters include large-scale vertical velocity at 500 mb and RH at several vertical levels.

https://doi.org/10.5194/gmd-2020-144
Preprint. Discussion started: 7 July 2020


Geoscientific Model Development Discussions

288
289 3.2 Offline calculation of cloud fraction
290 To evaluate the impact of assumptions of CF distributions for the RH- and PDF-
291 based schemes, we conducted offline calculations of the CF by using the reanalyzed
292 temperature, humidity, and condensate data from ERA-Interim. As the differences in
293 CF characteristics do not change from month to month, the results for July are shown
294 in Figure 2 as an example. The ERA-Interim reanalysis performed by Dee *et al*. [2011]
295 using a 0.75° resolution from 1979 to 2012 is used in the calculation. With this offline
296 approach, we can observe the impacts of these macrophysics assumptions with a
297 balanced atmospheric state provided by the reanalysis.
298 Overall, the geographical distributions from the two GTS schemes are similar to that
299 of the ERA-Interim reanalysis shown in Figure 2. In July, high clouds corresponding to
300 deep convection are shown over South and East Asia where monsoons prevail. The
301 diagnosed clouds of the GTS scheme have a maximum level of 125 hPa, which is
302 consistent with those of the ERA-Interim reanalysis, but also have a more extensive
303 cloud coverage of up to 90%. Below the freezing level at approximately 500 hPa, the
304 CF diagnosed by the GTS scheme is comparable with that diagnosed by ERA-Interim
305 reanalysis. The most substantial differences in CF between the GTS scheme and the
306 ERA-Interim are observed in the mixed-phase clouds, such as the low clouds over the
307 Southern and Arctic Oceans. Such differences suggest that more complexity in
308 microphysics assumptions may be needed to describe the large-scale balance of mixed-
309 phase clouds. The diagnosed CF for the Park macrophysics scheme is also shown in the
310 right column of Figure 2. We found that the cloud field diagnosed by the Park
311 macrophysics scheme was considerably different from that diagnosed by ERA-Interim
312 reanalysis and the GTS schemes. The Park scheme diagnosed overcast high clouds of
313 100–125 hPa with coverage of up to 100% over the warm pool and Intertropical
314 Convergence Zone, but very little cloud coverage below 200 hPa, suggesting that the
315 assumptions of the Park scheme are probably not suitable for large-scale states of the
316 ERA-Interim reanalysis.
317 However, such a calculation does not account for the feedback of the clouds to the
318 atmospheric states through condensation or evaporation and cloud radiative heating.
319 Therefore, we further extended our single-column CAM5.3 experiments to examine the
320 impact of the cloud PDF assumption.
321
322
323 4. Single-column results
324 This section presents the analysis of single-column simulations using the TWP-ICE
325 field campaign. We focused on the CF fields and humidity fields, and their relation to

https://doi.org/10.5194/gmd-2020-144
Preprint. Discussion started: 7 July 2020


Geoscientific Model Development Discussions

each other, to see how the RH_c assumption affects these features through humidity partitioning. Three sets of model experiments were conducted. In addition to the T_pdf of the GTS and Park schemes, we also include the T_pdf of the GTS scheme with the Slingo ice CF parameterization. This experiment can help us to interpret the impacts of RH_c on liquid and ice CFs separately.

Figure 3 shows the correlation between CF and RH for the three time periods during the TWP-ICE. As expected, the correlation coefficients are quite similar for the individual schemes during the active monsoon period when convective clouds dominated (R = 0.688, Park, vs. 0.698, T_pdf). In contrast, the correlation coefficient between CF and RH differs during the suppressed monsoon period when stratiform clouds dominated (R = 0.510, Park, vs. 0.728, T_pdf). The correlation coefficient between CF and RH is approximately 20% higher for the stratiform-cloud-dominated period when using T_pdf in the GTS scheme. It is also worth mentioning that, during the monsoon break period when both convective and stratiform clouds co-exist, the usage of the GTS scheme can also increase the correlation between CF and RH by 10% compared to the default Park scheme. The higher correlation coefficient for stratiform-cloud-dominated areas also suggests that the GTS scheme can somehow better simulate the variation of CF associated with RH, for which stratiform cloud macrophysics parameterization normally takes effect in CAM5.3.

Comparisons between T_pdf with the Slingo ice CF and the Park scheme can be used to examine the role of applying a PDF-based approach in simulating the liquid CF in the GTS scheme. The use of a PDF-based approach for calculating the liquid CF can increase the correlation between CF and RH by approximately 13% during the suppressed monsoon period (R = 0.637, T_pdf with Slingo, vs. 0.51, Park). Such an outcome also suggests that implementing a PDF-based approach for liquid clouds can lead to more reasonable fluctuations between CF and RH in GCM grids.

It turns out that using the PDF-based approach for ice clouds also contributes to the increased correlation between CF and RH by approximately 10%, as shown in Figure 3 with the T_pdf scheme (R = 0.637, T_pdf with Slingo, vs. 0.728, T_pdf). Such results also suggest that extending this PDF-based approach for ice clouds can better simulate changes in the cloud ice fraction using an RH-based approach rather than an RH_c-based approach. Such pair comparisons (*i.e.*, T_pdf with Slingo cloud ice fraction scheme vs. T_pdf and vs. Park) also reveal the important features of the GTS scheme, such as how variations in both the ice and liquid CF are better correlated with changes in RH of the GCM grids when compared to that of the default cloud macrophysics scheme.

Figure 4 shows scatter plots of RH and CF between 50 and 300 hPa determined from observations [Xie *et al.*, 2010] and simulated by models run for the suppressed monsoon period from the TWP-ICE case. It is evident that the relationship between CF and RH

https://doi.org/10.5194/gmd-2020-144
Preprint. Discussion started: 7 July 2020


Geoscientific Model Development Discussions

appears to be more linear using the T_pdf of the GTS scheme as shown in Figure 4(c) when compared to the default Park scheme (Figure 4(b)). Moreover, the CF-RH distributions simulated by the GTS scheme are also closer to those of the observational results except under more overcast conditions (*i.e.*, RH > 70% and RH > 110%). Similar to the results shown in Figure 3, the role of a PDF-based treatment of CF for the liquid CF can increase the degree of linearity between CF and RH (Figures 4(b) vs. 4(d)). On the other hand, by excluding PDF-based treatment for the cloud ice fraction in the GTS scheme, a more obvious spread in the CF-RH distribution is produced (comparing Figures 4(c) and 4(d)). In other words, results from the paired comparisons shown in Figure 4 are consistent with features shown in Figure 3, suggesting that applying a PDF-based treatment for both liquid and ice CF parameterization can indeed increase the linearity between CF and RH simulated by GCMs.

5. Global-domain results

5.1 Impacts on cloud fields

a. Cloud fraction

In Figure 5, total CF simulated by the GTS schemes and the CESM default cloud macrophysics scheme, obtained from the COSP satellite simulator of the AMWG package of NCAR CESM, are compared with the total CF in CALIPSO-GOCCP. Both global mean and root-mean-square error (RMSE) values are improved by applying U_pdf in the GTS scheme. The CF simulation resulting from the use of U_pdf in the GTS scheme is qualitatively similar to that of CloudSat/CALIPSO, especially over the mid- and high-latitude regions and for the annual and December-January-February (DJF) simulations (Figure 6). On the other hand, the results of the Park scheme in the tropics show clouds at higher altitudes than either U_pdf or T_pdf, in closer agreement with CloudSat/CALIPSO. Cross-section comparison of the zonal height shows that the CF simulation using U_pdf and T_pdf in the GTS scheme agrees better with that of CloudSat/CALIPSO than that produced by Park under most scenarios (globally, within 60° N–60° S, and within 30° N–30° S), especially for the annual and DJF simulations (Table 1). In contrast, some scenarios show lower RMSEs when the Park scheme is used, *e.g.*, for the June-July-August (JJA) season globally, within 30–90° N, and within 30–90° S. Interestingly, when high latitudes are included (*i.e.*, 30–90° N and 30–90° S), U_pdf still results in the smallest RMSE values, except for during the JJA season.

We also compared the annual latitude–longitude distributions of CF at different specific pressure levels (Figure 7). The use of U_pdf resulted in a CF simulation relatively similar to that of CloudSat/CALIPSO for mid-level clouds, *i.e.*, 300–700 mb, particularly for the mid- and high latitudes. However, none of the CF parameterizations

https://doi.org/10.5194/gmd-2020-144
Preprint. Discussion started: 7 July 2020


Geoscientific Model Development Discussions

are able to simulate stratocumulus clouds effectively, as revealed at the 850 and 900 mb levels. For high clouds, the GTS and Park schemes exhibit observable differences regarding the maximum CF level. Table 2 summarizes the RMSE values for the latitude–longitude distribution of CFs at nine specific levels for the three schemes and CloudSat/CALIPSO for the annual, JJA, and DJF means. For the annual mean, U_pdf results in the smallest RMSE at all levels except at 125 mb, for which the Park scheme yields the smallest RMSE (Table 2). For JJA, the Park scheme is closer to the observations aloft (100–200 mb) and nearest the surface (900 mb). For DJF, U_pdf again performs best at most levels except 100 and 125 mb, for which T_pdf is slightly better, while for JJA, U_pdf is only best for most of the levels below 300 mb. Overall, U_pdf in the GTS scheme results in better latitude–longitude CF distributions for 300–900 mb for the annual, DJF, and JJA means, suggesting improvements in CF simulation for middle and low clouds.

When annual, DJF, and JJA mean vertical CF profiles are averaged over the entire globe and between 30° N and 30° S, U_pdf in the GTS scheme can produce a global simulation close to that of CloudSat/CALIPSO for 200–850 mb (Figure S3). In contrast, there is a large discrepancy between the simulated and observed CFs over the tropics. Although the GTS schemes can simulate CF profiles above 100 mb, the height of the maximum CF is lower than that of CloudSat/CALIPSO. In contrast, the height of the maximum CF simulated by the Park scheme is similar to that of CloudSat/CALIPSO but overestimated in CF. As before, when compared with CloudSat/CALIPSO, U_pdf in the GTS scheme results in the smallest RMSE and the largest correlation coefficient of the three schemes, whether or not the lower levels are included except in JJA at 125 mb, for which Park yields the smallest RMSE (Table 3). The reason for excluding the lower levels from the statistical results is that there may be a bias for low clouds retrieved by CloudSat due to radar-signal blocking by deep convective clouds.

The different degrees of changes for the global and tropical CFs can be attributed to the relative roles of cumulus parameterizations (both deep and shallow) and stratus cloud macrophysics/microphysics for the different latitudinal regions. It is expected that the GTS scheme can alter CF simulations in the mid- and high-latitude areas more than in the tropics because more stratiform clouds occur in those areas. It is also interesting to note that, although it is known that more convective clouds exist in the tropics (*i.e.*, the cumulus parameterization contributes more to the grid CF), the GTS scheme can also affect the CF simulation over the tropics to some extent. Such different responses in GCMs can be attributed to the degree of correlation between CF and RH for the different types of clouds, as shown in the single-column model simulations (Figure 3). This increase in the correlation coefficient between CF and RH is also evident in the global simulations shown in Figure 8, where the two selected grids in the tropics are

https://doi.org/10.5194/gmd-2020-144
Preprint. Discussion started: 7 July 2020


Geoscientific Model Development Discussions

examined. It is clear that the correlation coefficient (R^2) is approximately 20% higher for high clouds when applying T_pdf or U_pdf in the GTS scheme rather than using the default Park scheme (R^2 = 0.410, Park, vs. 0.652, T_pdf, vs. 0.646, U_pdf). An increase in linearity between CF and RH with regard to high clouds can also be seen for other latitudinal grids, as shown in Figures S1 and S2, especially for the high latitudinal grids (Figure S3, R^2 = 0.265, Park, vs. 0.656, T_pdf, vs. 0.587, U_pdf). As addressed in Section 4, this increase in the correlation coefficient between CF and RH, also seen in the global simulation results, is contributed by the application of the PDF-based approach for parameterizing both the liquid and ice CFs in the GTS scheme.

b. Cloud fraction and cloud water content

In Figures 9 and 10, the distributions of CWC and CF as functions of large-scale vertical velocity at 500 mb (ω500) or mean RH averaged between 300 and 1000 mb (RH300–1000) are evaluated against CloudSat/CALIPSO observations for 30° N–30° S and 60° N–60° S. Figures 9 and 10 show that the model simulations are all qualitatively more similar to each other than to the observations. Further statistical comparisons are shown in Table 4. It is encouraging to note that, in addition to the slight improvements in CF for both of these latitudinal ranges, the use of U_pdf in the GTS scheme results in a CWC simulation that is more consistent with CloudSat/CALIPSO, whether it is plotted against ω500 or RH300–1000. The RMSE and correlation coefficient (R) values in Table 4 confirm this. For global simulations, using U_pdf also results in better agreement with CloudSat/CALIPSO for both CF and CWC when they are plotted against ω500, although for CWC plotted against RH300–1000, the Park scheme yields the smallest RMSE (Table 4). Overall, these comparisons yield results that are consistent with the general characteristics of most CMIP5 models, as found by Su *et al*. [2013]. GCMs in general simulate the distribution of cloud fields better with respect to a dynamical parameter as opposed to a thermodynamic parameter.

It is also worth noting that the use of U_pdf yields a 20–30% improvement in R when plotted against RH300–1000 for the two latitudinal ranges, 30° N–30° S and 60° N–60° S. The observable improvement in a thermodynamic parameter is an indication of the uniqueness of this GTS scheme, in that it is capable of simulating the variation in cloud fields relative to that in RH fields. There are also slight improvements in cloud fields with respect to large-scale dynamical parameters. On the other hand, the Park scheme results in an approximately 20% improvement in R when plotted against RH300–1000 for the global domain, suggesting that the default Park scheme still simulates cloud fields better over the high latitudinal regions. It is thus worth addressing the likelihood that the different CF and CWC results for the different latitudinal ranges simulated using the GTS scheme induce cloud–radiation interactions distinct from

https://doi.org/10.5194/gmd-2020-144
Preprint. Discussion started: 7 July 2020

those simulated in the Park scheme. Such changes in cloud–radiation interactions would not only modify the thermodynamic fields but also the dynamic fields in the GCMs. These changes are in turn likely to affect the climate mean state and variability. We assess and compare these potential effects in the following subsection.

5.2 Effects on annual mean climatology

GTS schemes tend to produce smaller RMSE values for most of the global mean values of the radiation flux, cloud radiative forcing, and CF parameters shown in Table 5, suggesting that the GTS scheme is capable of simulating the variability of these variables. Furthermore, the assumed U_pdf shape appears to perform better for outgoing longwave radiation flux, longwave cloud forcing (LWCF), and CF at various levels, whereas the T_pdf assumption is better for simulating net and shortwave radiation flux at the top of the atmosphere as well as shortwave cloud forcing (SWCF) (Table 5). On the other hand, the Park scheme is better for simulating clear-sky net shortwave radiation flux and precipitation. Smaller RMSE values can also be seen for parameters such as total precipitable water, total-column cloud liquid water, zonal wind at 200 mb (hereafter, U_200), and air temperature at 200 mb (hereafter, T_200) when U_pdf of GTS is used. For global annual means, U_pdf simulates net radiation flux at the top of the atmosphere, all- and clear-sky outgoing longwave radiation flux, and precipitable water as well as U_200 and T_200 in closer agreement with observations. In contrast, the Park scheme is better for simulating global mean variables such as net shortwave radiation flux at the top of the atmosphere, longwave cloud forcing, and precipitation. T_pdf simulates SWCF closest to the observational mean.

Overall, the averaged RMSE values of the ten parameters are 0.97 and 0.96 for U_pdf and T_pdf, respectively, in the GTS schemes (Figure 11), suggesting that using the GTS schemes would result in global simulation performances more or less similar to those from the Park scheme. It is also worth noting that the biases in RH are smallest when U_pdf in the GTS scheme is used (Table S1 of the supplementary material). In contrast, T_pdf results in the smallest biases for SWCF, sea-level pressure, and ocean rainfall within 30° N–30° S. On the other hand, the Park scheme produces the smallest biases regarding mean fields such as LWCF, land rainfall within 30° N–30° S, Pacific surface stress within 5° N–5° S, zonal wind at 300 mb, and temperature.

Comparisons of latitude–height cross-sections of RH and ERA-Interim show that the GTS schemes tend to simulate RH values smaller than the default scheme does, especially for high-latitude regions (> 60° N and 60° S), as shown in Figure 12. In general, in terms of RH, using T_pdf in the GTS scheme results in better agreement with ERA-Interim (Table 6). Figure 13 shows that the Park and T_pdf schemes are wetter than ERA-Interim almost everywhere and that the uniform scheme is sometimes

https://doi.org/10.5194/gmd-2020-144
Preprint. Discussion started: 7 July 2020


Geoscientific Model Development Discussions

drier. Table 7(a) further suggests that specific humidity simulated by the GTS schemes is slightly more consistent with ERA-Interim than the Park scheme. Comparisons of air temperature show that the three schemes tend to have cold biases almost everywhere. However, it is interesting to note that the cold biases are reduced to some extent while using the GTS schemes compared to the default scheme, as is evident in the smaller values of RMSE shown in Table 7(b). These effects on moisture and temperature are likely to result in changes in the annual cycle and seasonality of climatic parameters. Such observable changes in RH, clouds (both CF and CWC), and cloud forcing suggest that the GTS scheme will simulate cloud macrophysics processes in GCMs quite differently from the Park scheme, owing to the use of a variable-width PDF that is determined based on grid-mean information.

5.3 Changes in the annual cycle of climatic variables

Figure 14 shows the annual cycle of precipitable water simulated by the three schemes. The magnitude of precipitable water simulated by the GTS schemes is closer to the ERA-Interim data than the Park simulation is (Table 8). Interestingly, U_pdf results in slightly better agreement with ERA-Interim than T_pdf for the region 60° N–60° S. This implies that the GTS scheme would alter the moisture field for both RH and precipitable water in GCMs. These results are relatively more realistic with respect to both the moisture field and CF and CWC (Figures 9 and 10) and are likely to yield a more reasonable cloud–radiation interaction in the GCMs. It is therefore also worth examining any differences in dynamic fields, for example, in the annual U_200 cycle, between the three schemes and the ERA-Interim data (Figure 15). Like the annual cycle of precipitable water, U_200 simulated by the GTS schemes is closer to that of ERA-Interim than that simulated by the Park scheme, as supported by the smaller RMSE shown in Table 8. Furthermore, the U_pdf assumption results in a better annual U_200 cycle than the T_pdf assumption, especially for 60° N–60° S. This further supports the argument that this GTS scheme can effectively modulate global simulations, with respect to both thermodynamic and dynamical climatic variables.

Figure 16 displays the global mean annual cycles of several parameters simulated by the three schemes and the corresponding parameters from observational data. The GTS scheme simulations of total precipitable water (TMQ) are close to that of ERA-Interim; indeed, U_pdf almost exactly reproduces the ERA-Interim TMQ. However, we must admit that such good agreement of the global mean is partly due to offsetting wet and dry differences from ERA-Interim. The GTS schemes also produce a more reasonable global mean annual cycle for outgoing longwave radiation (FLUT). It is probably due to the reduced CF simulated by the GTS scheme compared to the Park scheme even though the cloud top heights simulated by GTS are lower than observations in the

https://doi.org/10.5194/gmd-2020-144
Preprint. Discussion started: 7 July 2020


Geoscientific Model Development Discussions

554 tropics. Interestingly, for SWCF, T_pdf yields a simulation closer to the observations
555 than the other two schemes, which is consistent with the features of the global annual
556 mean of SWCF shown in Figure 11 and Table S1. However, for LWCF, the annual cycle
557 simulated by Park is closest to the observations. The U_pdf of the GTS scheme also
558 results in improvements in U_200 and T_200 (Figure 16). The RMSEs for all of these
559 comparisons confirm these results (Table 9).
560
561 5.4 Changes in cloud–radiation interactions
562 As mentioned in Section 5.1, usage of the GTS cloud macrophysics schemes would
563 affect the cloud fields, *i.e.*, CF and CWC. This, in turn, is likely to affect global
564 simulations with respect to both mean climatology and the annual cycles of many
565 climatic parameters (as discussed in Sections 5.2 and 5.3) through cloud–radiation
566 interactions. Figure 17 compares CF, radiation heating rate (*i.e.*, longwave heating rate
567 plus shortwave heating rate, hereafter QRL+QRS) and temperature trends due to moist
568 processes (hereafter, DTCOND) for each pair-wise combination of the three schemes.
569 Qualitatively consistent changes in CF are apparent for the GTS schemes, *e.g.*, an
570 increase in the highest clouds over the tropics and a decrease below them, a decrease in
571 150–400 mb clouds over the mid-latitudes, a decrease in 300–700 mb clouds over the
572 high latitudes, an increase in 300–700 mb clouds over the tropics to mid-latitudes, and
573 an increase in low clouds over the high-latitude regions. The GTS schemes also yield a
574 significant increase in CF at atmospheric levels higher than 300 mb over the high-
575 latitude regions (Figure 17). These changes affect the radiation calculations to some
576 extent. In addition, CWC is also affected by the GTS schemes (Figures 9 and 10). The
577 combined effects of the changes in CF and CWC are likely to result in changes in cloud–
578 radiation interactions. In addition, although there are significant changes in CF at high
579 atmospheric levels in the high-latitude regions, the combined effect of CF and CWC on
580 QRL+QRS is quite small, owing to the low CWC values over this region. The changes
581 in moisture processes, *i.e.*, DTCOND (Figure 17), also suggest that the combined
582 effects of the changes in the thermodynamic and dynamical fields occur as a result of
583 changes in cloud–radiation interactions within the GCMs from GTS schemes.
584 The bottom panel in Figure 17 shows the differences in CF, QRL+QRS, and
585 DTCOND between the two GTS schemes. Relative to T_pdf, U_pdf simulates a greater
586 CF for 300–1000 mb clouds within 60° N–60° S, but a smaller CF for all three cloud
587 levels for the high-latitude regions. Furthermore, the CWC vertical cross-section also
588 differs for the two GTS schemes (data not shown for limitations of space). Combining
589 the changes in CF and CWC, the corresponding changes in QRL+QRS and DTCOND,
590 particularly the increase of low clouds over the mid-latitude region, are clear with an
591 obvious decrease of high clouds over the tropical to mid-latitude region.

https://doi.org/10.5194/gmd-2020-144
Preprint. Discussion started: 7 July 2020


Geoscientific Model Development Discussions

592 Observable changes in large-scale circulations are likely, given the various changes
593 in QRL+QRS and DTCOND resulting from applying different cloud macrophysics.
594 Accordingly, both the mean and variability of the climate simulated by the GCMs differ
595 among the three schemes, as shown in the previous subsections. These results
596 emphasize the importance of improving cloud-related parameterization to provide
597 better simulations of the cloud–radiation interaction within GCMs. Furthermore, as
598 previously shown, the cloud–radiation interaction is highly sensitive to the assumptions
599 of the CF parameterization used in the macrophysical scheme in the GCMs, even if
600 there is only a small change in the CF parameterization. The uniqueness of the GTS
601 scheme is in its application of a variable PDF width to calculate CF in the default PDF-
602 based CF scheme of the CESM model. Further systematic experiments are necessary to
603 improve our understanding of the sensitivity of the GTS scheme, and some are
604 presented in Section 5.6.
605
606 5.5 Consistent changes in cloud radiative forcing, cloud fraction, and cloud condensates
607 Observable changes in clouds and radiation fluxes after adopting the GTS scheme
608 were clearly shown in the previous subsections. It is thus worth examining features in
609 cloud radiative forcings caused by the GTS scheme that produce such changes, as
610 compared to those of the default Park scheme. Figure 18 shows the difference in total
611 cloud fraction, SWCF, LWCF, CF, and averaged cloud water contents, as well as the
612 averaged RH at the three levels i.e., 100–400, 400–700, and 700–1000 mb, derived
613 from the T_pdf of GTS with the Park results subtracted. One can readily observe that
614 changes in SWCF (Figure 18(b)) are quite consistent with those for total CF, showing
615 a decrease in the total CF over the area within 30° N and 30° S with an increase
616 everywhere else (Figure 18(a)). Such prominent changes in latitudinal distribution of
617 SWCF can be further related to the changes in the low (Figure 18(e)) and middle (Figure
618 18(f)) CFs particularly associated with low clouds.
619 On the other hand, changes in the high CF (Figure 18(d)) are also quite consistent
620 with those in LWCF (Figure 18(c)), showing an overall decrease of high clouds
621 especially over the tropical convection areas. As expected, changes in cloud water
622 condensates (Figures 18(g)–(i)) are closely related to changes in the CF at the three
623 levels except for the middle clouds. Therefore, according to the evidence shown in
624 Figures 18(a)–(i), it is clear that use of the GTS scheme would cause significant changes
625 in the spatial distribution of low, middle, and high clouds (both in CF and cloud water
626 condensates) that would result in corresponding changes in cloud radiative forcings
627 (both for SWCF and LWCF).
628 Surprisingly, changes in RH at the three levels (Figures 18(j)–(l)) are relatively less
629 consistent with changes in the CF and condensates, especially for middle and low

https://doi.org/10.5194/gmd-2020-144
Preprint. Discussion started: 7 July 2020


Geoscientific Model Development Discussions

clouds over the mid- and high-latitude areas. Such results also indicate that there are complicated factors accounting for changes in RH in the GCMs. We suggest that, in addition to the active roles of the GTS scheme in redistributing/modulating moisture between clouds (*i.e.*, cloud liquid or ice) and environment (water vapor) in GCM grids, thermodynamic and dynamical feedback resulting from cloud–radiation interactions also contribute to RH changes. At the present stage, we cannot quantify these individual contributions. More in-depth analysis is needed to unveil the detailed mechanisms of why GTS schemes tend to produce less low clouds over the tropics while more low clouds over the mid- and high latitudes compared to the default Park scheme, as well as observable changes regarding middle and high clouds.

5.6 Uncertainty in GTS cloud fraction parameterization

a. Assumption of PDF shape in the GTS scheme

In general, the simulations of CF, RH, and other parameters (*e.g.*, global annual mean and/or annual cycle) using the T_pdf scheme that have been discussed and illustrated thus far have distribution features qualitatively and values quantitatively between those of the Park and U_pdf schemes. In other words, the characteristics of the T_pdf simulations are a combination of those from both the default Park scheme and the U_pdf scheme. This is to be expected because there are fewer differences between the Park and T_pdf schemes than between the Park and U_pdf schemes in terms of cloud macrophysics parameterization. Since the shape of the PDF is triangular for both the Park and T_pdf schemes, the only difference between these two is that T_pdf has a variable PDF width that is based on the grid-mean mixing ratio of hydrometeors and the saturation ratio of the atmospheric environment, rather than the fixed-width function of RH_c. Even such a minor difference, however, can have an impact on both the thermodynamic and dynamical fields in global simulations. Our findings further suggest that the use of a variable PDF width to determine CF results in some changes in consistency between the RH and CF fields, as well as in the simulation of SWCF and net radiation flux at the top of atmosphere. As mentioned in Section 1, a diagnostic approach to determining the triangular PDF width of the default Park scheme can be used to refine the Park scheme [Appendix A of Park *et al*., 2014]. This is effectively the same as using the GTS scheme with T_pdf.

However, it is also evident that assuming a uniform PDF (*i.e.*, a rectangular shape) can have a larger effect on global simulations, as seen with our use of U_pdf. It is interesting to note that the use of U_pdf yields a smaller overall RMSE for many thermodynamic and dynamical fields than does the use of T_pdf. This implies that a uniform distribution is probably more appropriate for the 2° horizontal resolution currently used in global simulations. The scale-dependence of the PDF shape is

https://doi.org/10.5194/gmd-2020-144
Preprint. Discussion started: 7 July 2020


Geoscientific Model Development Discussions

668 certainly important to consider, as revealed in our comparisons between T_pdf and
669 U_pdf, but this is beyond the scope of this paper. Furthermore, the possible dependence
670 of PDF shape on specific cloud systems in different regions should also be examined
671 using systematic tests and simulation designs.
672
673 b. Uncertainty resulting from cloud-ice fraction parameterization
674 It is worth evaluating the possible uncertainty related to CF for cloud ice because the
675 saturation adjustment assumption used for cloud liquid may not apply to cloud ice, as
676 discussed in Section 1. We thus examine the sensitivity of the super-saturation values
677 for the cloud ice fraction by multiplying by q_{si}, as shown in equation 4 by the constant
678 *sup*. Several values of *sup* are assumed for the cloud ice fraction in the GTS schemes
679 with CF simulated using Slingo's approach to parameterization as used by Park *et al*.
680 [2014] and are compared with the CloudSat/CALIPSO observational data (Figure S4).
681 Both GTS schemes are sensitive to the *sup* value. For U_pdf, CF decreases more-or-
682 less linearly with increasing *sup* values, but there is no such clear linearity for T_pdf,
683 especially for *sup* values of 1.0000–1.0005. Interestingly, changing the *sup* value for
684 the cloud ice fraction affects the cloud liquid fraction results for the scheme. We also
685 find that the CF profile simulated by U_pdf when *sup* = 1.0005 is similar to that
686 simulated using Slingo's approach to parameterization, especially for middle and low
687 clouds. Based on these sensitivity tests, it is evident that the *sup* value used in the cloud
688 ice fraction formulae of the GTS scheme can be regarded as a tunable parameter under
689 the present cloud macrophysics and microphysics framework of the CESM model.
690 When *sup* = 1.0 in the GTS scheme with U_pdf, the results are comparable to
691 CloudSat/CALIPSO observations, while with T_pdf, the *sup* value can be tuned
692 between 1.0 and 1.005 to mimic the CloudSat/CALIPSO data (Figure S4). Thus, the
693 results of GTS schemes are sensitive to the supersaturation threshold and suggest that
694 it is still quite challenging to produce a reasonable parameterization for the cloud ice
695 fraction, given the longer time-scales needed for ice clouds to reach saturation
696 equilibrium.
697
698 6. Conclusions
699 In this paper, we presented a macrophysics parameterization based on a probability
700 density function (PDF) called the GFS-TaiESM-Sundqvist (GTS) cloud macrophysics
701 scheme, which is based on Sundqvist's cloud macrophysics concept for global models
702 and the recent modification of the cloud macrophysics in the NCAR CESM model by
703 Park *et al*. [2014]. The GTS scheme especially excludes the assumption of a prescribed
704 critical relative humidity threshold (RH_c), which is included in the default cloud
705 macrophysics schemes, by determining the width of the PDF based on grid

https://doi.org/10.5194/gmd-2020-144
Preprint. Discussion started: 7 July 2020


Geoscientific Model Development Discussions

706 hydrometeors and saturation ratio.

707 We first used ERA-Interim reanalysis data to examine offline the validity of the
708 relationship between cloud fraction (CF) and relative humidity (RH) based on the PDF
709 assumption. Results showed that the GTS assumption better describes the large-scale
710 equilibrium between CF and environment conditions. In a single-column model setup,
711 we noticed several improved characteristics of the CF and humidity in the model
712 simulation when the *ad hoc* RH_c assumptions were removed. First, the CF-RH
713 relationship is more consistent in our modified scheme and an overall increase in
714 linearity between CF and RH of approximately 20% was observed, especially for
715 stratiform clouds. Second, according to the pair-wise comparisons shown and discussed
716 in Figures 3 and 4, the use of PDF-based treatments for parameterizing both liquid and
717 ice CFs in the GTS schemes contributed to the linear CF-RH relationship.

718 According to our detailed comparisons with observational cloud field data (CF and
719 cloud water content (CWC)) from CloudSat/CALIPSO, GTS parameterization is able
720 to simulate changes in CF that are associated with changes in RH in global simulations.
721 Improvements with respect to the CF of middle clouds, the boreal winter, and mid- and
722 high latitudes are particularly evident. Furthermore, examination of the vertical
723 distributions of CF and CWC as a function of large-scale dynamical and
724 thermodynamic parameters suggests that, compared to the default scheme, simulations
725 of CF and CWC from the GTS scheme are qualitatively more consistent with the
726 CloudSat/CALIPSO data. It is particularly encouraging to observe that the GTS scheme
727 is also capable of substantially increasing the pattern correlation coefficient of CF and
728 CWC as a function of a large-scale thermodynamic parameter (*i.e.*, RH300–1000).
729 These effects appear to have a substantial impact on global climate simulations via
730 cloud–radiation interactions.

731 The fact that CF and CWC simulated by the GTS scheme are temporally and spatially
732 closer to those of the observational data suggests that not only the climatological mean
733 but also the annual cycles of many parameters would be better simulated by the GTS
734 cloud macrophysical scheme. Improvements with respect to thermodynamic fields such
735 as upper-troposphere and lower-stratosphere temperature, RH, and total precipitable
736 water were more substantial even than those in the dynamical fields. This was
737 consistent with our comparisons based on the vertical distribution of CF and CWC as
738 functions of large-scale dynamical and thermodynamic forcing. Interestingly, the GTS
739 scheme results in observable changes in the annual cycle of zonal wind at 200 hPa,
740 which suggests that the modification of thermodynamic fields resulting from changes
741 in cloud–radiation interactions will, in turn, reciprocally affect the dynamical fields.
742 Accordingly, it is worth investigating possible changes in large-scale circulation,
743 monsoon evolution, and short- and long-term climate variability in future research.

https://doi.org/10.5194/gmd-2020-144
Preprint. Discussion started: 7 July 2020

GTS schemes can simulate spatial distributions of cloud radiative forcings (both for shortwave and longwave) quite differently compared to the default Park scheme. Changes in cloud radiative forcings are very consistent with different latitudinal changes in CF and cloud water condensates at the three cloud levels. The most important feature of the GTS scheme is that CF is self-consistently determined based on hydrometeors and the environmental information in the model grid box in the general circulation model (GCM) simulation. In contrast to the prescribed vertical profile of RH_c used in many current GCMs, the width of the PDF in the GTS scheme is variable and calculated in a diagnostic way. A fixed RH_c is thus no longer used once clouds are formed. This feature also potentially makes the GTS scheme a candidate macrophysics parameterization for use in modern global weather forecasting and climate prediction models as it better simulates the CF-RH relationship. However, further efforts are required to develop a more meaningful and physical way to parameterize the super-saturation ratio assumption applied to the cloud ice fraction in the GTS scheme, and to investigate why a uniform PDF in the GTS scheme performs better overall than the triangular PDF.

References

Austin, R. T., Heymsfield, A. J., and Stephens, G. L.: Retrieval of ice cloud microphysical parameters using the CloudSat millimeter-wave radar and temperature, J. Geophys. Res., 114, D00A23, doi:10.1029/2008JD010049, 2009.

Bogenschutz, P. A., Gettelman, A., Morrison, H., Larson, V. E., Craig, C., and Schanen, D. S.: Higher-Order Turbulence Closure and Its Impact on Climate Simulations in the Community Atmosphere Model, J. Climate, 26, 9655–9676, doi: 10.1175/JCLI-D-13-00075.1, 2013.

Bogenschutz, P. A., Gettelman, A., Morrison, H., Larson, V. E., Schanen, D. P., Meyer, N. R., and Craig, C.: Unified parameterization of the planetary boundary layer and shallow convection with a higher-order turbulence closure in the Community Atmosphere Model, Geosci. Model Dev., 5, 1407–1423, 2012.

Bogenschutz, P. A., and Krueger, S. K.: A simplified pdf parameterization of subgrid-scale clouds and turbulence for cloud-resolving models, Journal of Advances in Modeling Earth Systems, 5 (2), 195–211, doi:10.1002/jame.20018, 2013.

Boucher, O., Randall, D., Artaxo, P., Bretherton, C., Feingold, G., Forster, P., Kerminen, V.-M., Kondo, Y., Liao, H., Lohmann, U., Rasch, P., Satheesh, S.K., Sherwood, S., Stevens, B. and Zhang, X. Y.: Clouds and Aerosols. In: Climate Change 2013: The Physical Science Basis. Contribution of Working Group I to the Fifth Assessment Report of the Intergovernmental Panel on Climate Change [Stocker, T. F., D. Qin,

https://doi.org/10.5194/gmd-2020-144
Preprint. Discussion started: 7 July 2020

782 G.-K. Plattner, M. Tignor, S. K. Allen, J. Boschung, A. Nauels, Y. Xia, V. Bex and P.
783 M. Midgley (eds.)], Cambridge University Press, Cambridge, United Kingdom and
784 New York, NY, USA, 2013.
785 Bougeault, P.: Modeling the trade-wind cumulus boundary layer. Part II: A higher-order
786 one-dimensional model, J. Atmos. Sci., 38, 2429–2439, 1981.
787 Chaboureau, J.-P., and Bechtold, P.: A Simple Cloud Parameterization Derived from
788 Cloud Resolving Model Data: Diagnostic and Prognostic Applications, J. Atmos.
789 Sci., 59, 2362–2372, 2002.
790 Chosson, F., Vaillancourt, P. A, Milbrandt, J. A., Yau, M. K., and Zadra, A.: Adapting
791 Two-Moment Microphysics Schemes across Model Resolutions: Subgrid Cloud and
792 Precipitation Fraction and Microphysical Sub–Time Step, J. Atmos. Sci., 71, 2635–
793 2653, doi: 10.1175/JAS-D-13-0367.1, 2014.
794 Dee, D. P., Uppala, S. M., Simmons, A. J., Berrisford, P., Poli, P., Kobayashi, S., Andrae,
795 U., Balmaseda, M. A., Balsamo, G., Bauer, P., Bechtold, P., Beljaars, A., van de Berg,
796 L., Bidlot, J., Bormann, N., Delsol, C., Dragani, R., Fuentes, M., Geer, A. J.,
797 Haimberger, L., Healy, S. B., Hersbach, H., Hólm, E. V., Isak-sen, L., Kallberg, P.,
798 Köhler, M., Matricardi, M., McNally, A.P., Monge-Sanz, B. M., Morcrette, J.-J.,
799 Park, B. K., Peubey, C.,de Rosnay, P., Tavolato, C., Thépaut, J.-N., and Vitart, F.:
800 TheERA-Interim reanalysis: configuration and performance of the data assimilation
801 system, Q. J. Roy. Meteorol. Soc., 137, 553–597, doi:10.1002/qj.828, 2011.
802 Donner, et al.: The Dynamical Core, Physical Parameterizations, and Basic Simulation
803 Characteristics of the Atmospheric Component AM3 of the GFDL Global Coupled
804 Model CM3, J. Clim., 24, 3484–3519, doi: 10.1175/2011JCLI3955.1, 2011.
805 Firl, G. J.: A Study of Low Cloud Climate Feedbacks Using a Generalized Higher-
806 Order Closure Subgrid Model, PhD Dissertation, Department of Atmospheric
807 Science, Colorado State University, 253pp, 2013.
808 Firl, G. J., and Randall, D. A.: Fitting and Analyzing LES Using Multiple Trivariate
809 Gaussians, J. Atmos. Sci., 72, 1094–1116, 2015.
810 Franklin, C. N., Jakob, C., Dix, M., Protat, A., and Roff, G.: Assessing the performance
811 of a prognostic and a diagnostic cloud scheme using single column model
812 simulations of TWP–ICE, Q. J. R. Meteorol. Soc., 138, 734–754. doi:10.1002/qj.954,
813 2012.
814 Golaz, J.-C., Horowitz, L. W., and Levy, II H.: Cloud tuning in a coupled climate model:
815 impact on 20th century warming, Geophys. Res. Lett., 40, 2246–2251,
816 doi:10.1002/grl.50232, 2013.
817 Golaz, J., Larson, V., and Cotton, W.: A PDF-based model for boundary layer clouds:
818 Part 1. Method and model description, J. Atmos. Sci., 59 (24), 3540–3551, 2002.
819 Hogan, R. J, O'Connor, E. J., and Illingworth, A. J.: Verification of cloud fraction

https://doi.org/10.5194/gmd-2020-144
Preprint. Discussion started: 7 July 2020

forecasts, Q. J. R. Meteorol. Soc., 135, 1494–1511, 2009.

Hourdin, F., Mauritsen, T., Gettelman, A., Golaz, J.-C., Balaji, V., Duan, Q., Folini, D., Ji, D., Klocke, D., Qian, Y., Rauser, F., Rio, C., Tomassini, L., Watanabe, M., and Williamson, D.: The art and science of climate model tuning, Bulletin of the American Meteorological Society, published online, doi: 10.1175/BAMS-D-15-00135.1, 2016.

Jakob, C., and Klein, S. A.: A parameterization of the effects of cloud and precipitation overlap for use in general circulation models, Quart. J. Roy. Meteor. Soc., 126, 2525–2544, doi:10.1002/qj.49712656809, 2000.

Kay, J. E., Hillman, B., Klein, S., Zhang, Y., Medeiros, B., Gettelman, G., Pincus, R., Eaton, B., Boyle, J., Marchand, R. and Ackerman, T.: Exposing global cloud biases in the Community Atmosphere Model (CAM) using satellite observations and their corresponding instrument simulators, J. Climate, 25, 5190–5207. doi: http://dx.doi.org/10.1175/JCLI-D-11-00469.1, 2012.

Larson, V. E., Golaz, J.-C., and Cotton, W. R.: Small-scale and mesoscale variability in cloudy boundary layers: Joint probability density functions, J. Atmos. Sci., 59, 3519–3539, 2002.

Lee, W.-L., Wang, Y.-C., Shiu, C.-J., Tsai, I., Tu, C.-Y., Lan, Y.-Y., Chen, J.-P., Pan, H.-L., and Hsu, H.-H.: Taiwan Earth System Model Version 1: Description and Evaluation of Mean State, Geosci. Model Dev. Discuss., https://doi.org/10.5194/gmd-2019-377, in review, 2020.

Li, J.-L. F., Waliser, D. E., Chen, W.-T., Guan, B., Kubar, T. L., Stephens, G. L., Ma, H.-Y., Min, D., Donner, L. J., Seman, C. J., and Horowitz, L. W.: An observationally-based evaluation of cloud ice water in CMIP3 and CMIP5 GCMs and contemporary reanalyses using contemporary satellite data, J. Geophys. Res., doi:10.1029/2012JD017640, 2012.

Lin, Y.: Humidity variability revealed by a sounding array and its implications for cloud representation in GCMs, J. Geophys. Res. Atmos., 119, 10,499–10,514, doi:10.1002/2014JD021837, 2014.

Marchand, R., Mace, G. G., Ackerman, T., and Stephens, G.: Hydrometeor Detection Using Cloudsat–An Earth-Orbiting 94-GHz Cloud Radar, J. Atmos. Oceanic Technol., 25, 519–533, 2008.

Mauritsen, T., et al.: Tuning the climate of a global model, J. Adv. Model. Earth Syst., 4, M00A01, doi:10.1029/2012MS000154, 2012.

May, P. T., Mather, J. H., Vaughan, G., Jakob, C., McFarquhar, G. M., Bower, K. N., and Mace,G. G.: The Tropical Warm Pool International Cloud Experiment, Bull. Amer. Meteor. Soc., 89, 629–645, 2008.

McCoy, D. T., Tan, I., Hartmann, D. L., Zelinka, M. D., and Storelvmo, T.: On the

https://doi.org/10.5194/gmd-2020-144
Preprint. Discussion started: 7 July 2020

relationships among cloud cover, mixed-phase partitioning, and planetary albedo in GCMs, J. Adv. Model. Earth Syst., 8, 650–668, doi:10.1002/2015MS000589, 2016.

Molod, A.: Constraints on the Profiles of Total Water PDF in AGCMs from AIRS and a High-Resolution Model, J. Climate, 25, 8341–8352, 2012.

Neale, R. B. et al.: Description of the NCAR Community Atmosphere Model (CAM 5.0), NCAR technical note (NCAR/TN-486+STR), National Center For Atmospheric Research Boulder, Colorado, USA, 2010.

Neale R. B. et al.: The Mean Climate of the Community Atmosphere Model (CAM4) in Forced SST and Fully Coupled Experiments, J. Climate, 26, 5150–5168, doi: 10.1175/JCLI-D-12-00236.1, 2013.

Park, R.-S., Chae, J.-H., and Hong, S.-Y.: A Revised Prognostic Cloud Fraction Scheme in a Global Forecasting System, Mon. Wea. Rev., 144, 1219–1229, doi: 10.1175/MWR-D-15-0273.1, 2016.

Park, S., Bretherton, C. S., and Rasch, P. J.: Integrating Cloud Processes in the Community Atmosphere Model, Version 5, J. Climate, 27, 6821–6856, 2014.

Park, S.: A unified convection scheme (UNICON). Part I: Formulation, J. Atmos. Sci., 71, 3902–3930, 2014a.

Park, S.: A unified convection scheme (UNICON). Part II: Simulation, J. Atmos. Sci., 71, 3931–3973, 2014b.

Qian, Y., Long, C. Wang, N., H., Comstock, J. M., McFarlane, S. A., and Xie, S.: Evaluation of cloud fraction and its radiative effect simulated by IPCC AR4 global models against ARM surface observations, Atmos. Chem. Phys., 12, 1785–1810, doi:10.5194/acp-12-1785-2012, 2012.

Quaas, J.: Evaluating the “critical relative humidity” as a measure of subgrid-scale variability of humidity in general circulation model cloud cover parameterizations using satellite data, J. Geophys. Res., 117, D09208, doi:10.1029/2012JD017495, 2012.

Rasch, P. J., and Kristjansson, J. E.: A comparison of the CCM3 model climate using diagnosed and predicted condensate parameterizations, J. Climate, 11, 1587–1614, doi:10.1175/1520-0442(1998)011,1587:ACOTCM.2.0.CO;2, 1998.

Roeckner, E., et al.: The atmospheric general circulation model ECHAM-4: Model description and simulation of present-day climate, Rep. 218, 90 pp., Max Planck Institute for Meteorology, Hamburg, Germany, 1996.

Salzmann, M., Ming, Y., Golaz, J. C., Ginoux, P. Morrison, A., Gettelman, H., A., Krämer, M., and Donner, L. J.: Two-moment bulk stratiform cloud microphysics in the GFDL AM3 GCM: Description, evaluation, and sensitivity tests, Atmos. Chem. Phys., 10, 8037–8064, doi:10.5194/acp-10-8037-2010, 2010.

Schmidt, G. A., et al.: Configuration and assessment of the GISS ModelE2

https://doi.org/10.5194/gmd-2020-144
Preprint. Discussion started: 7 July 2020

contributions to the CMIP5 archive, J. Adv. Model. Earth Syst., 6, 141–184, doi:10.1002/2013MS000265, 2014.

Slingo, J. M.: The development and verification of a cloud prediction scheme for the ECMWF model, Quart. J. Roy. Meteor. Soc., 113, 899–927, doi:10.1002/qj.49711347710, 1987.

Smith, R.: A scheme for predicting layer clouds and their water content in a general circulation model, Quart. J. Roy. Meteor. Soc., 116, 435–460, doi:10.1002/qj.49711649210, 1990.

Sommeria, G., and Deardorff, J. W.: Subgrid-scale condensation in models of nonprecipitating clouds, J. Atmos. Sci., 34, 344–355, 1977.

Sotiropoulou, G., Sedlar, J., Forbesb, R., and Tjernstrom, M.: Summer Arctic clouds in the ECMWF forecast model: an evaluation of cloud parameterization schemes, Q. J. R. Meteorol. Soc., doi:10.1002/qj.2658, (2015).

Storer, R. L., Griffin, B. Hoft, M., J., Weber, J. K., Raut, E., Larson, V. E., Wang, M., and Rasch, P. J.: Parameterizing deep convection using the assumed probability density function method, Geosci. Model. Dev., 8 (1), 1–19, doi:10.5194/gmd-8-1-2015, 2015.

Su, H., et al.: Diagnosis of regime-dependent cloud simulation errors in CMIP5 models using “A-Train” satellite observations and reanalysis data, J. Geophys. Res. Atmos., 118, 2762–2780, doi:10.1029/2012JD018575, 2013.

Sundqvist, H.: Parameterization of condensation and associated clouds in models for weather prediction and general circulation simulation, Physically Based Modeling and Simulation of Climate and Climatic Change, M. E. Schlesinger, Ed., Kluwer Academic, 433–461, 1988.

Sundqvist, H., Berge, E., and Kristjansson, J. E.: Condensation and cloud parameterization studies with a mesoscale numerical weather prediction model, Mon. Wea. Rev., 117, 1641–1657, doi:10.1175/15200493(1989)117, 1989.

Tiedtke, M.: Representation of clouds in large-scale models, Mon. Wea. Rev., 121, 3040–3061, doi:10.1175/1520-0493(1993)121,3040: ROCILS.2.0.CO;2, 1993.

Tompkins, A. M.: A prognostic parameterization for the subgrid-scale variability of water vapor and clouds in large-scale models and its use to diagnose cloud cover, J. Atmos. Sci., 59, 1917–1942, doi:10.1175/1520-0469(2002)059, 2002.

Tompkins, A. M.: The parametrization of cloud cover,ECMWF Moist Processes Lecture Note Series, p.available at http://www.ecmwf.int/newsevents/training/, 2005.

Tompkins, A. M., Gierens, K., and Rädel, G.: Ice supersaturation in the ECMWF integrated forecast system, Quart. J. Roy. Meteor. Soc., 133, 53–63, doi:10.1002/qj.14, 2007.

https://doi.org/10.5194/gmd-2020-144
Preprint. Discussion started: 7 July 2020

934 Wilson, D. R., Bushell, A. C., Kerr-Munslow, A. M., Price, J. D., Morcrette, C. J.: PC2:
935 A prognostic cloud fraction and condensation scheme. I: Scheme description, Q. J.
936 R. Meteorol. Soc 134: doi: 10.1002/qj.333, 2008a.
937 Wilson, D. R., Bushell, A. C., Kerr-Munslow, A. M., Price, J. D., Morcrette, C. J.,
938 Bodas-Salcedo, A.: PC2: A prognostic cloud fraction and condensation scheme. II:
939 Climate model simulations, Q. J. R. Meteorol. Soc. 134: 2109–2125, doi:
940 10.1002/qj.332, 2008b.
941 Xie, S., Hume, T., Jakob, C., Klein, S., McCoy, R., and Zhang, M.: Observed large-
942 scale structures and diabatic heating and drying profiles during TWP-ICE, J. Climate,
943 23, 57–79, 2010.
944 Xu, K. M., and Randall, D. A.: A semiempirical cloudiness parameterization for use in
945 climate models, J. Atmos. Sci., 53, 3084–3102, doi:10.1175/1520-
946 0469(1996)053,3084:ASCPFU.2.0.CO;2, 1996.
947 Zhang, M., Lin, W., Bretherton, C., Hack, J., and Rasch, P. J.: A modified formulation
948 of fractional stratiform condensation rate in the NCAR Community Atmospheric
949 Model (CAM2), J. Geophys. Res., 108(D1), 4035, doi:10.1029/2002JD002523,
950 2003.
951
952
953

https://doi.org/10.5194/gmd-2020-144
Preprint. Discussion started: 7 July 2020

954
955 Code availability
956 The codes of the GTS scheme used in this study can be obtained from the following
957 website:
958 https://doi.org/10.5281/zenodo.3626654
959
960
961 Author contributions. HHH is the initiator and primary investigator of the TaiESM
962 project. CJS developed code and wrote the majority of the paper. YCW also developed
963 code and wrote part of the paper. WTC helped process CloudSat/CALIPSO satellite
964 data. HLP and RS helped develop the theoretical basis of the GTS scheme. YHC helped
965 with the off-line calculations. CAC helped with most of the visualizations.
966
967
968 Competing interests. The authors declare that they have no conflict of interest.
969
970
971

https://doi.org/10.5194/gmd-2020-144
Preprint. Discussion started: 7 July 2020

Acknowledgements

We would like to dedicate this paper to Dr. Chia Chou in appreciation for his encouragement. The work is supported in part by the Ministry of Science and Technology (MOST), Taiwan (R.O.C.) under the projects MOST 100-2119-M-001-029-MY5 and 105-2119-M-002-028-MY3. This work is also part of the Consortium for Climate Change Study (CCliCs) – Laboratory for Climate Change Research. CloudSat data is available through Austin *et al*. [2009]. Other observations, satellite retrievals, and reanalysis data used in the paper were obtained from the AMWG diagnostic package provided by CESM, NCAR. Detailed information regarding those observational data are available at http://www.cgd.ucar.edu/amp/amwg/diagnostics/plotType.html. We would like to thank Anthony Abram (www.uni-edit.net) for editing and proofreading this manuscript.

https://doi.org/10.5194/gmd-2020-144
Preprint. Discussion started: 7 July 2020

Geoscientific Model Development Discussions

Table 1. Root-mean-square errors (RMSE) for comparisons of latitude–height cross-sections of CF among the three macrophysical schemes (Park: default scheme; T_pdf: triangular PDF in the GTS scheme; U_pdf: uniform PDF in the GTS scheme) and observational data from CloudSat/CALIPSO (Figure 6). Comparisons are made of the means for five latitudinal ranges and three periods (JJA: June, July, August; DJF: December, January, February). The smallest RMSE value of the three schemes in each case is bold and underlined.

	Global			60°N~60°S			30°N~30°S			30°N~90°N			30°S~90°S		
	Park	T_pdf	U_pdf	Park	T_pdf	U_pdf	Park	T_pdf	U_pdf	Park	T_pdf	U_pdf	Park	T_pdf	U_pdf
Annual	7.15	8.27	**6.75**	5.25	**4.53**	4.85	5.84	5.37	**5.05**	8.78	10.40	**8.52**	6.46	8.29	**6.18**
JJA	**7.40**	11.30	9.50	6.27	5.64	**5.61**	6.03	5.96	**5.56**	**8.91**	10.60	9.13	**6.93**	15.50	12.70
DJF	9.04	9.37	**6.99**	5.62	**5.24**	5.38	6.29	5.53	**5.36**	12.80	13.00	**10.00**	6.33	7.85	**3.82**

Table 2. RMSEs for comparisons between CF at nine pressure levels, as simulated by the three macrophysical schemes (Park, T_pdf, U_pdf) and observational data from CloudSat/CALIPSO (Figure 7). The comparisons are made for three periods (JJA: June, July, August; DJF: December, January, February). The smallest RMSE value of the three schemes in each case is bold and underlined.

	Annual			JJA			DJF		
	Park	T_pdf	U_pdf	Park	T_pdf	U_pdf	Park	T_pdf	U_pdf
100 mb	6.07	5.40	**4.71**	**4.85**	12.70	10.10	7.88	**3.94**	4.20
125 mb	**4.70**	5.56	4.80	**6.13**	12.60	10.10	5.96	**4.56**	4.81
200 mb	7.23	8.34	**6.78**	**9.80**	14.90	11.90	8.64	6.57	**6.46**
300 mb	10.80	9.63	**7.98**	11.60	12.90	**10.80**	12.40	11.70	**9.06**
400 mb	11.80	10.50	**6.93**	12.40	10.50	**9.55**	12.70	13.90	**8.06**
500 mb	11.00	11.50	**7.65**	11.90	10.60	**9.28**	11.70	13.40	**8.50**
700 mb	8.64	9.47	**8.19**	9.63	10.80	**9.46**	10.70	11.10	**9.41**
850 mb	14.30	14.20	**12.00**	14.80	15.40	**12.80**	16.10	15.30	**13.20**
900 mb	12.50	15.10	**12.30**	**13.30**	16.60	13.60	15.10	16.40	**12.90**

https://doi.org/10.5194/gmd-2020-144
Preprint. Discussion started: 7 July 2020

Geoscientific Model Development Discussions
Open Access
EGU

Table 3. RMSEs and correlation coefficients (R, in brackets) for comparisons between the vertical CF profiles simulated by the three macrophysical schemes (Park, T_pdf, U_pdf) and observational data from CloudSat/CALIPSO (Figure S3). Comparisons are made for three periods (JJA: June, July, August; DJF: December, January, February) and two latitudinal ranges. The smallest RMSE value of the three schemes in each case is bolded and underlined.

		Global			30°N~30°S		
		Park	T_pdf	U_pdf	Park	T_pdf	U_pdf
Including low levels	Annual	8.03 (0.83)	9.51 (0.86)	**7.92** (0.87)	6.15 (0.60)	6.03 (0.53)	**5.38** (0.59)
	JJA	**8.58** (0.81)	11.52 (0.85)	9.66 (0.85)	6.61 (0.61)	6.06 (0.54)	**5.87** (0.62)
	DJF	9.14 (0.81)	10.20 (0.85)	**7.92** (0.86)	6.31 (0.59)	6.65 (0.52)	**5.60** (0.57)
Excluding low levels	Annual	5.97 (0.91)	6.51 (0.96)	**5.32** (0.99)	5.89 (0.63)	5.75 (0.51)	**5.13** (0.55)
	JJA	**6.60** (0.92)	9.39 (0.97)	7.72 (0.98)	6.13 (0.63)	6.22 (0.49)	**5.55** (0.58)
	DJF	6.05 (0.92)	6.76 (0.95)	**4.85** (0.99)	6.20 (0.60)	5.93 (0.49)	**5.45** (0.52)

Table 4. (a) RMSE and (b) R values for comparisons between CF and CWC simulated by the three macrophysical schemes (Park, T_pdf, and U_pdf) and plotted against vertical velocity at 500 mb (ω500) or averaged RH for 300–1000 mb (RH300–1000, obtained from the ERA-Interim reanalysis) and observational data from CloudSat/CALIPSO (Figures 9 and 10). The comparisons are made for three latitudinal ranges. The smallest RMSE or largest R value of the three schemes in each case is bolded and underlined.

(a)

RMSE		Global			60°N~60°S			30°N~30°S		
		Park	T_pdf	U_pdf	Park	T_pdf	U_pdf	Park	T_pdf	U_pdf
OMEGA@500 mb	CWC	11.10	10.90	**9.83**	11.40	11.20	**10.10**	14.10	13.80	**12.50**
	CF	7.65	7.26	**6.13**	7.55	7.23	**6.24**	8.13	8.07	**7.21**
RH@300-1000 mb	CWC	**8.73**	9.69	11.60	13.50	15.10	**11.80**	19.10	18.00	**12.00**
	CF	17.90	18.30	**13.90**	15.40	17.30	**12.70**	18.80	18.30	**12.90**

(b)

R		Global			60°N~60°S			30°N~30°S		
		Park	T_pdf	U_pdf	Park	T_pdf	U_pdf	Park	T_pdf	U_pdf
OMEGA@500 mb	CWC	0.73	0.77	**0.80**	0.74	0.77	**0.80**	0.60	0.66	**0.74**
	CF	0.84	0.85	**0.89**	0.85	0.85	**0.88**	0.83	0.82	**0.84**
RH@300-1000 mb	CWC	**0.64**	0.54	0.45	0.44	0.34	**0.62**	0.22	0.25	**0.55**
	CF	0.31	0.40	**0.59**	0.51	0.46	**0.68**	0.45	0.45	**0.66**

https://doi.org/10.5194/gmd-2020-144
Preprint. Discussion started: 7 July 2020

Geoscientific Model Development Discussions

Table 5. Global annual means (Mean) and RMSE values for comparisons with the observed values (Obs) for a selection of climatic parameters simulated by the three cloud macrophysical schemes (Park, T_pdf, and U_pdf). The smallest RMSE value or closest global mean of the three schemes in each case is bolded and underlined.

Parameters	Obs	Mean (Park)	Mean (T_pdf)	Mean (U_pdf)	RMSE (Park)	RMSE (T_pdf)	RMSE (U_pdf)
RESTOA_CERES-EBAF	0.81	4.18	3.25	**-1.06**	12.39	**10.43**	11.11
FLUT_CERES-EBAF	239.67	234.97	237.88	**238.14**	8.78	6.73	**6.50**
FLUTC_CERES-EBAF	265.73	259.06	259.65	**260.45**	7.55	7.12	**6.48**
FSNTOA_CERES-EBAF	240.48	**239.15**	241.14	237.08	13.97	**11.64**	12.79
FSNTOAC_CERES-EBAF	287.62	**291.26**	291.31	291.70	**7.08**	7.09	7.58
LWCF_CERES-EBAF	26.06	**24.10**	21.77	22.31	6.78	6.77	**6.21**
SWCF_CERES-EBAF	-47.15	-52.11	**-50.18**	-54.61	15.98	**12.90**	15.43
PRECT_GPCP	2.67	**2.97**	3.04	3.14	**1.09**	1.10	1.15
PREH2O_ERAI	24.25	25.64	24.90	**24.45**	2.56	2.05	**2.03**
CLDTOT_Cloudsat+CALIPSO	66.82	**64.11**	70.77	70.09	9.87	11.38	**9.76**
CLDHGH_Cloudsat+CALIPSO	40.33	38.17	44.79	**40.22**	9.37	9.28	**8.17**
CLDMED_Cloudsat+CALIPSO	32.16	27.22	30.41	**31.26**	8.03	6.95	**6.28**
CLDLOW_Cloudsat+CALIPSO	43.01	**43.63**	43.67	46.19	**12.78**	18.06	16.17
CLDTOT_CALIPSO GOCCP	67.25	56.43	55.45	**61.72**	14.38	15.37	**10.28**
CLDHGH_CALIPSO GOCCP	32.04	**25.57**	22.48	24.46	**9.04**	11.30	10.16
CLDMED_CALIPSO GOCCP	18.09	11.21	14.55	**18.19**	8.35	6.34	**6.02**
CLDLOW_CALIPSO GOCCP	37.95	33.24	33.16	**38.41**	10.63	11.33	**9.98**
TGCLDLWP(ocean)	79.87	42.55	40.68	**48.74**	40.92	42.37	**35.16**
U_200_MERRA	15.45	16.18	15.87	**15.66**	2.52	2.11	**1.94**
T_200_ERAI	218.82	215.58	215.76	**216.84**	4.03	3.37	**2.13**

Table 6. RMSEs for comparisons between the latitude–height cross-sections of RH simulated by the three macrophysical schemes (Park, T_pdf, and U_pdf) and ERA-Interim (Figure 12). The comparisons are made for three periods (JJA: June, July, August; DJF: December, January, February) and two latitudinal ranges. The smallest RMSE value of the three schemes in each case is bolded and underlined.

RH	Park	T_pdf	U_pdf
Annual	11.2	**6.4**	9.4
JJA	11.2	**7.3**	10.1
DJF	11.8	**6.9**	9.7

https://doi.org/10.5194/gmd-2020-144
Preprint. Discussion started: 7 July 2020

Geoscientific Model Development Discussions

Table 7. RMSEs for comparisons between the latitude–height cross-sections of (a) specific humidity q and (b) air temperature T simulated by the three macrophysical schemes (Park, T_pdf, and U_pdf) and ERA-Interim (Figure 13). The comparisons are made for three periods (JJA: June, July, August; DJF: December, January, February) and two latitudinal ranges. The smallest RMSE value of the three schemes in each case is bolded and underlined.

(a)

q	Park	T_pdf	U_pdf
Annual	0.29	0.25	**0.23**
JJA	0.32	**0.26**	0.27
DJF	0.29	0.27	**0.25**

(b)

T	Park	T_pdf	U_pdf
Annual	2.62	2.49	**2.05**
JJA	2.65	2.43	**2.24**
DJF	2.94	2.86	**2.60**

Table 8. RMSEs for comparisons between the annual cycles of zonal mean total precipitable water (TMQ) and annual cycles of zonal wind at 200 mb (U200) simulated by the three macrophysical schemes (Park, T_pdf, and U_pdf) and ERA-Interim (Figures 14 and 15).

	Park	T_pdf	U_pdf
TMQ	1.44	0.86	**0.82**
U200	1.97	1.74	**1.49**

https://doi.org/10.5194/gmd-2020-144
Preprint. Discussion started: 7 July 2020

Geoscientific Model Development Discussions
Open Access
EGU

Table 9. RMSEs for comparisons between the global mean annual cycles of several parameters simulated by the three macrophysical schemes (Park, T_pdf, and U_pdf) and corresponding observational data (Figure 16). The smallest RMSE value of the three schemes in each case is bolded and underlined.

	Park	T_pdf	U_pdf
TMQ	2.08	**1.70**	1.74
FLUT	8.15	6.71	**6.31**
LWCF	6.18	6.32	**6.06**
SWCF	14.00	**11.80**	14.00
U_200	2.34	2.04	**1.70**
T_200	5.57	4.50	**2.55**

https://doi.org/10.5194/gmd-2020-144
Preprint. Discussion started: 7 July 2020

Geoscientific Model Development
Discussions
Open Access
EGU

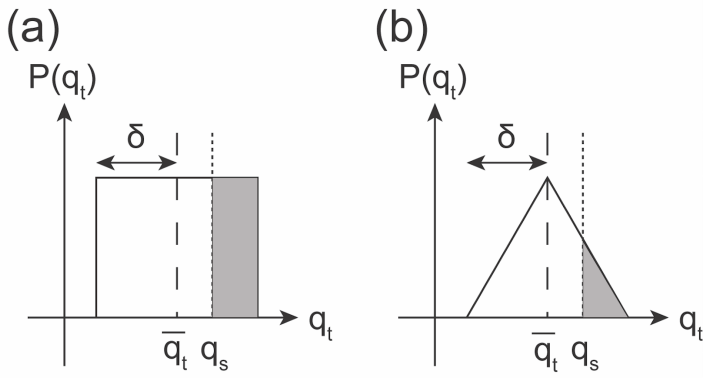

Figure 1. Illustration of sub-grid PDF of total water substance q_t with (a) uniform distribution and (b) triangular distribution. The shaded part shows the saturated cloud fraction, δ represents the width of the PDF, $\overline{q_t}$ denotes the grid-mean value of total water substance, and q_s represents the saturation mixing ratio as the temperature is assumed to be uniform within the grid.

https://doi.org/10.5194/gmd-2020-144
Preprint. Discussion started: 7 July 2020

Geoscientific Model Development
Discussions
Open Access
EGU

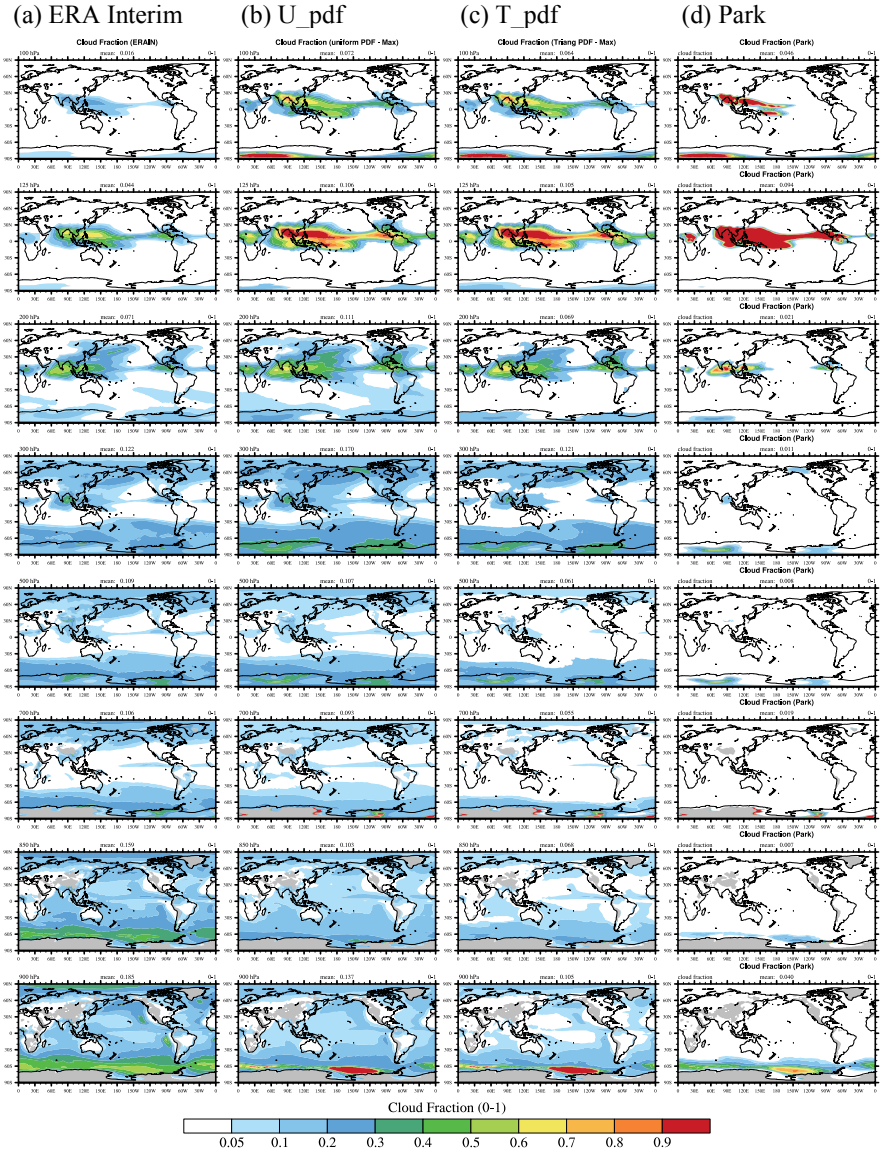

Figure 2. Mean cloud fraction in July (a) from the ERA-Interim reanalysis dataset and (b, c, d) diagnosed from cloud fraction schemes, with temperature, moisture, and condensates from the ERA-Interim reanalysis provided. From left to right, these schemes are the (b) U_pdf, (c) T_pdf, and (d) Park macrophysics schemes. Cloud distributions from 100 to 900 hPa are plotted from top to bottom.

https://doi.org/10.5194/gmd-2020-144
Preprint. Discussion started: 7 July 2020

Geoscientific Model Development
Discussions
Open Access
EGU

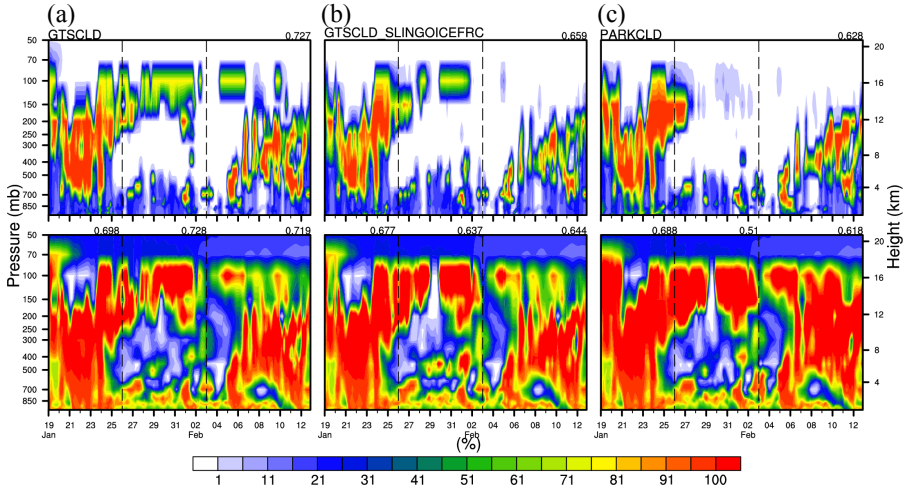

Figure 3. Pressure–time cross-sections of cloud fraction (upper row) and relative humidity (lower row) simulated by the three different cloud macrophysical schemes; (a) T_pdf, (b) T_pdf with Slingo ice cloud fraction scheme, and (c) the Park scheme during the TWP-ICE field campaign.

https://doi.org/10.5194/gmd-2020-144
Preprint. Discussion started: 7 July 2020

Geoscientific Model Development Discussions

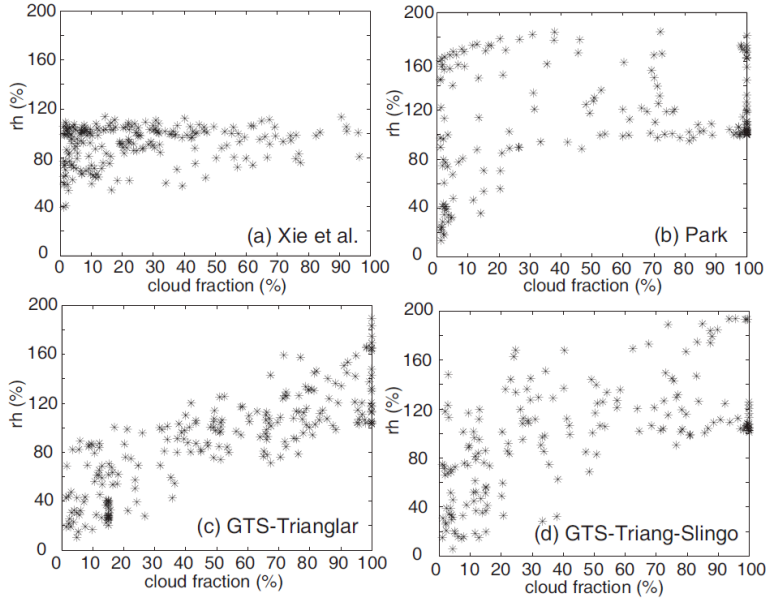

Figure 4. Scatter plots of high-level (50–300 hPa) relative humidities and cloud fractions during the suppressed monsoon period of the TWP-ICE field campaign (26 January to 2 February, 2006) observed by (a) Xie *et al*. [2010] and simulated by SCAM with the (b) Park of CAM5.3, (c) T_pdf, and (d) T_pdf with Slingo ice cloud macrophysics schemes.

https://doi.org/10.5194/gmd-2020-144
Preprint. Discussion started: 7 July 2020

Geoscientific Model Development
Discussions
Open Access
EGU

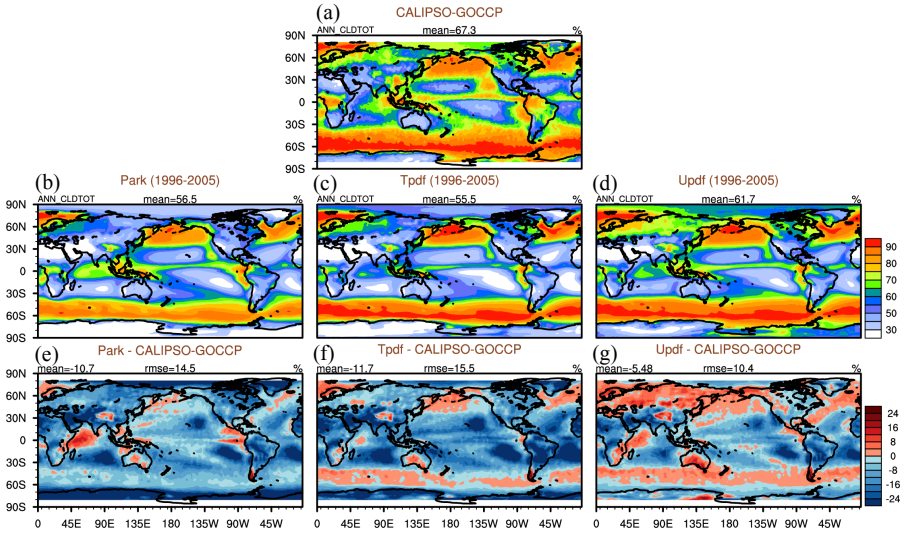

Figure 5. Total cloud fraction (CF) from (a) CALIPSO-GOCCP and simulated by the three schemes: (b) the default Park, (c) T_pdf, and (d) U_pdf, using the COSP satellite simulator of the NCAR CESM model. Differences between the simulated and observed total CFs derived from (e) the default Park, (f) T_pdf, and (g) U_pdf schemes.

https://doi.org/10.5194/gmd-2020-144
Preprint. Discussion started: 7 July 2020

Geoscientific Model Development Discussions
Open Access
EGU

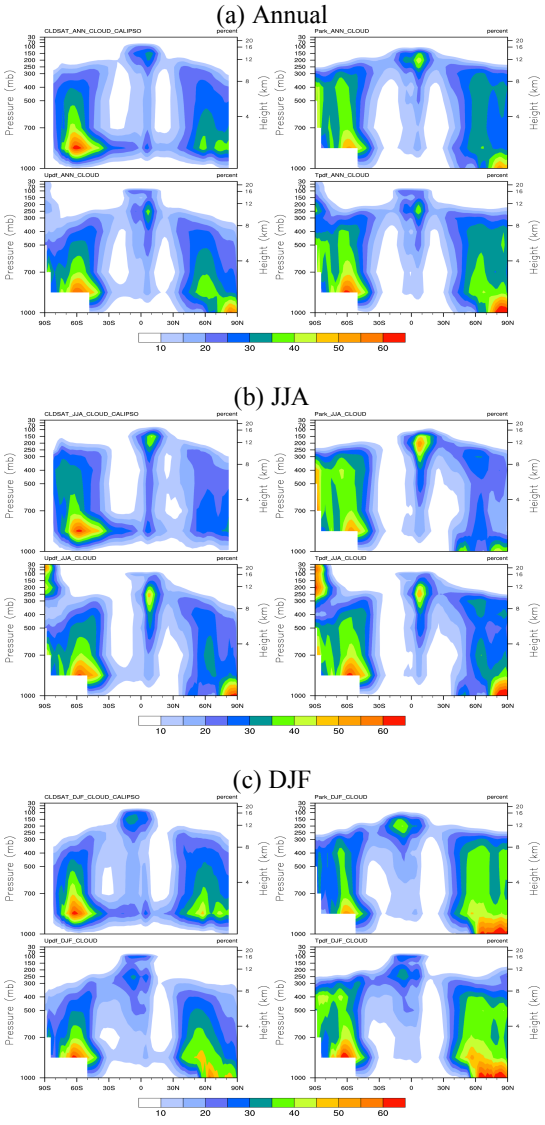

Figure 6. Latitude–height cross-sections of (a) annual, (b) June-July-August (JJA), and (c) December-January-February (DJF) mean CFs from CloudSat/CALIPSO data (upper left) and the the Park (upper right), U_pdf (lower left), and T_pdf (lower right) schemes.

https://doi.org/10.5194/gmd-2020-144
Preprint. Discussion started: 7 July 2020

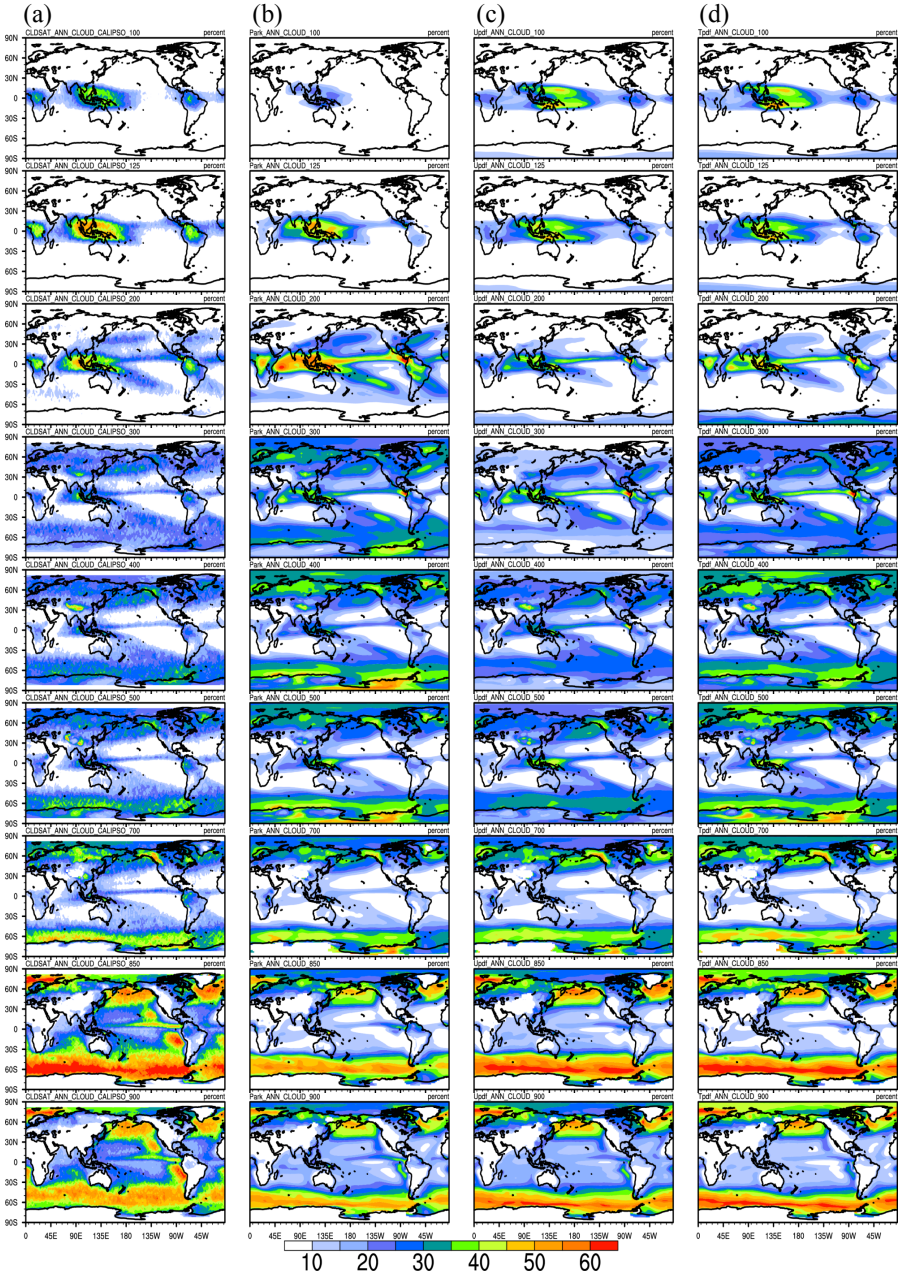

Figure 7. CFs at nine pressure levels (one pressure level per row; top to bottom: 100, 125, 200, 300, 400, 500, 700, 850, and 900 mb) from (a) CloudSat/CALIPSO observational data and simulated by (b) the default Park, (c) U_pdf, and (d) T_pdf schemes.

https://doi.org/10.5194/gmd-2020-144
Preprint. Discussion started: 7 July 2020

Geoscientific Model Development Discussions
Open Access
EGU

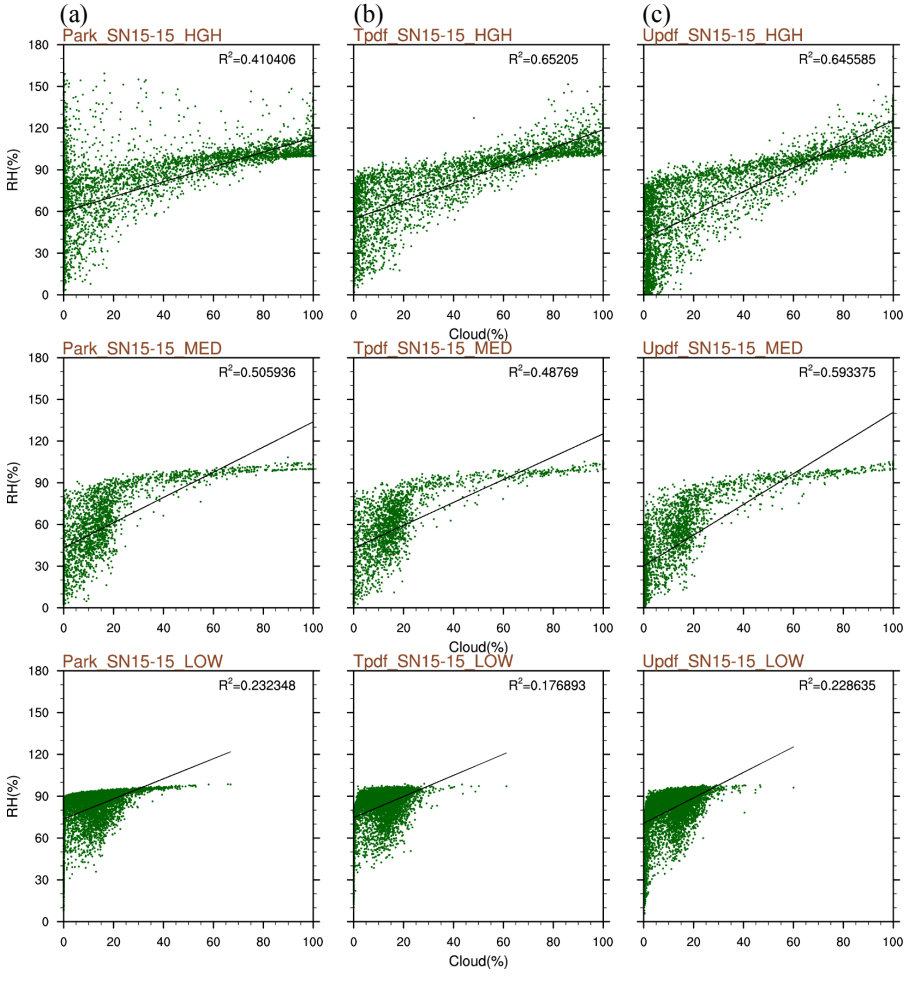

Figure 8. CF versus RH at three cloud levels (top to bottom: high, middle, and low clouds) simulated by (a) the default Park, (b) T_pdf, and (c) U_pdf schemes. Daily data of the two grid points ((180° E, 15° N) and (180° E, 15° S)) from 1999 to 2000 are used to generate the scatter plots, and linear regression lines with correlation coefficients are also shown.

https://doi.org/10.5194/gmd-2020-144
Preprint. Discussion started: 7 July 2020

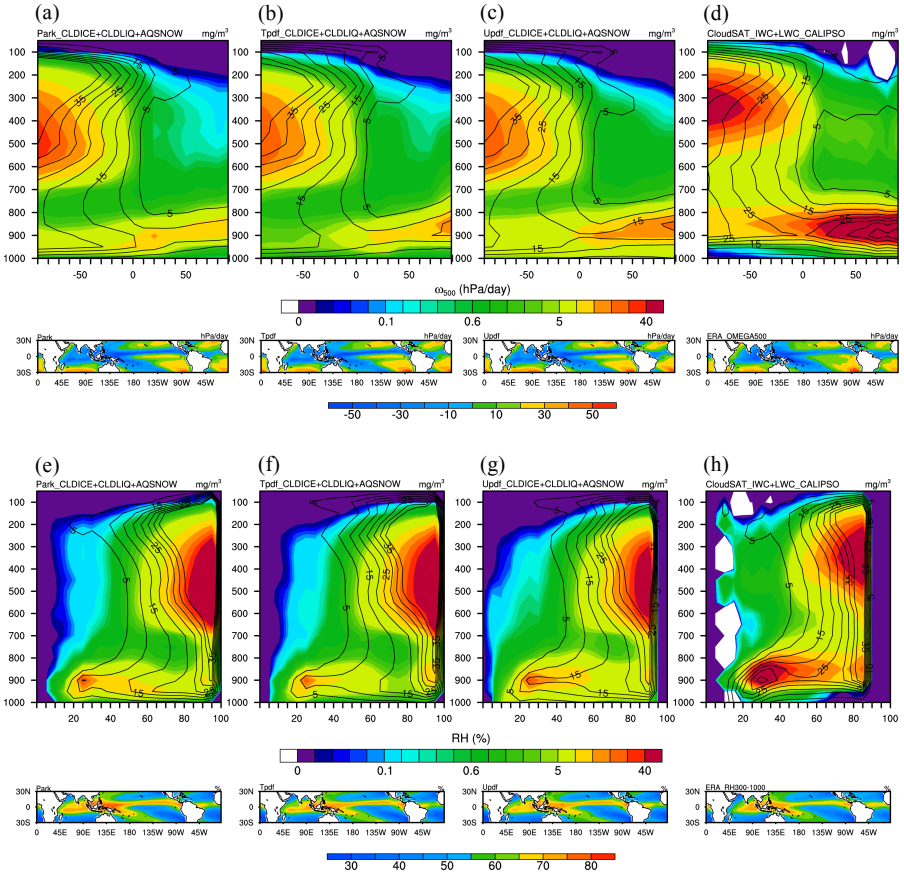

Figure 9. Vertical distribution of CF (contour lines) and CWC (colors) as functions of two large-scale parameters: vertical velocity at 500 mb (ω500, upper eight panels) and relative humidity averaged between 300 and 1000 mb (RH300–1000, lower eight panels) for the latitudinal range 30° N–30° S. Columns present simulations by the (a, e) Park, (b, f) T_pdf, and (c, g) U_pdf schemes, and (d, h) observational data from CloudSat/CALIPSO.

https://doi.org/10.5194/gmd-2020-144
Preprint. Discussion started: 7 July 2020

Geoscientific Model Development
Discussions
Open Access
EGU

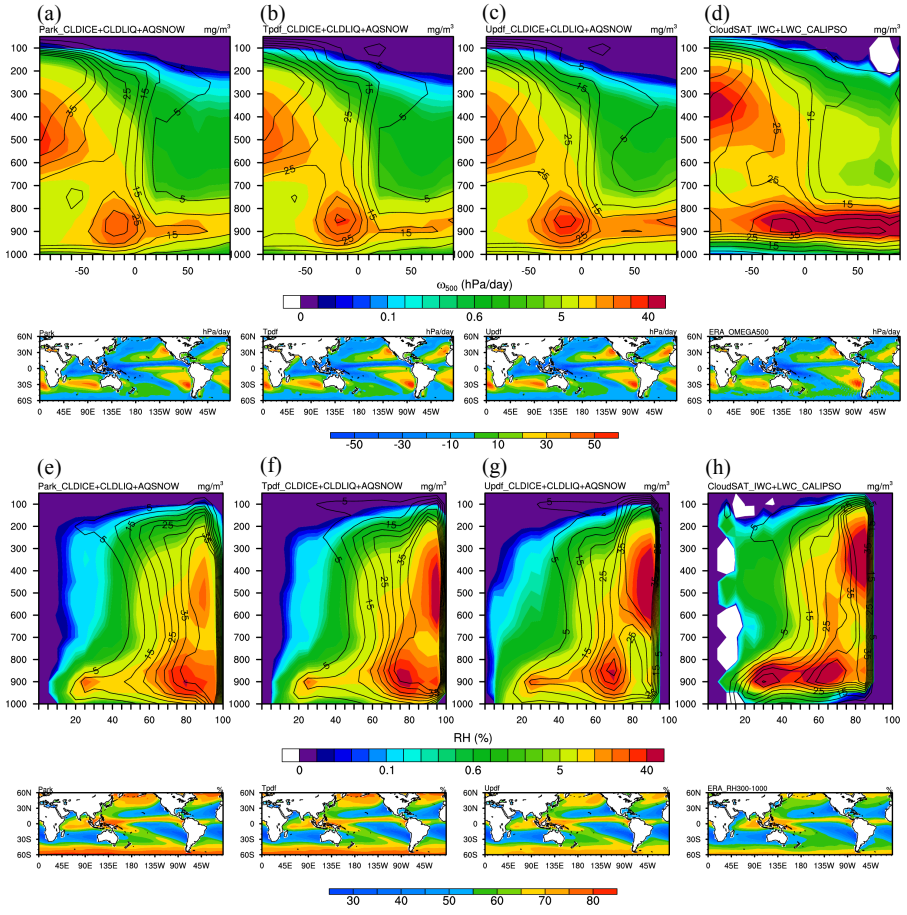

Figure 10. Vertical distribution of CF (contour lines) and CWC (colors) as functions of two large-scale parameters: ω500 (upper eight panels) and RH300–1000 (lower eight panels) for the latitudinal range 60° N–60° S. Columns present simulations by the (a, e) Park, (b, f) T_pdf, and (c, g) U_pdf, and (d, h) observational data from CloudSat/CALIPSO.

https://doi.org/10.5194/gmd-2020-144
Preprint. Discussion started: 7 July 2020

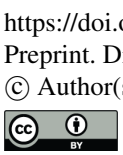

Geoscientific Model Development
Discussions
Open Access
EGU

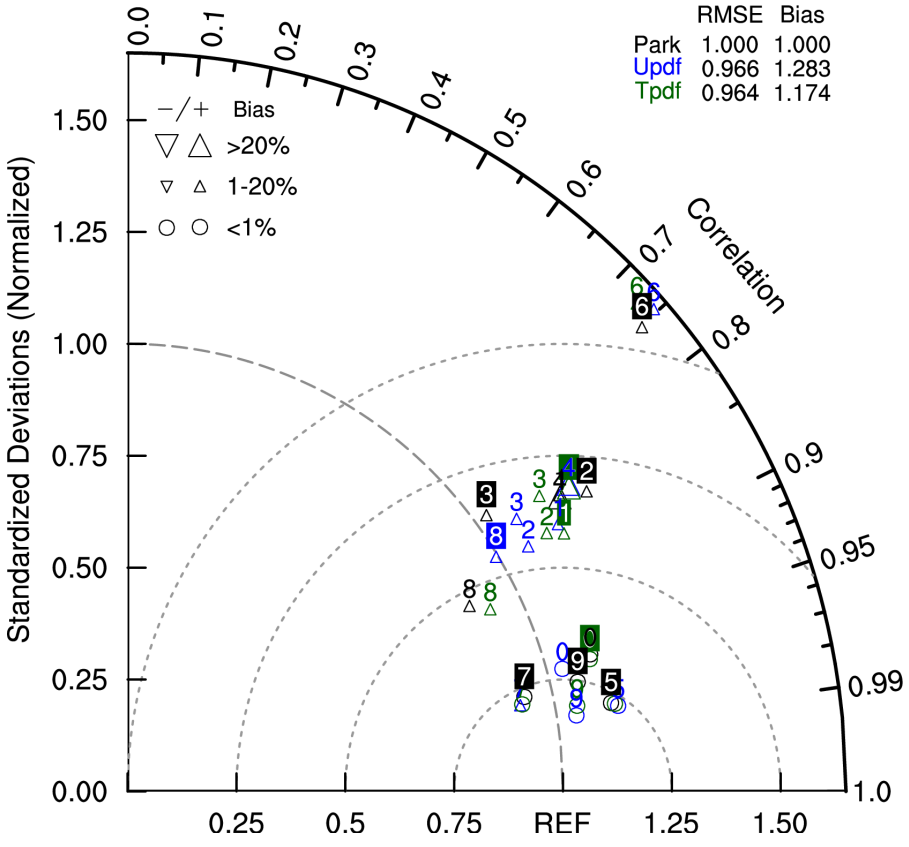

Figure 11. Space–time Taylor diagram for the ten climatic parameters simulated by the three macrophysical schemes (Park: black symbols; U_pdf: green; T_pdf: blue) and comparisons of these with the corresponding observational data provided by the atmospheric diagnostic package from the NCAR CESM group. The ten climatic parameters are marked from 0 to 9 where 0 denotes sea level pressure; 1 is SW cloud forcing, 2 is LW cloud forcing, 3 is land rainfall, 4 is ocean rainfall, 5 is land 2-m temperature, 6 is Pacific surface stress, 7 is zonal wind at 300 mb, 8 is relative humidity, and 9 is temperature.

https://doi.org/10.5194/gmd-2020-144
Preprint. Discussion started: 7 July 2020

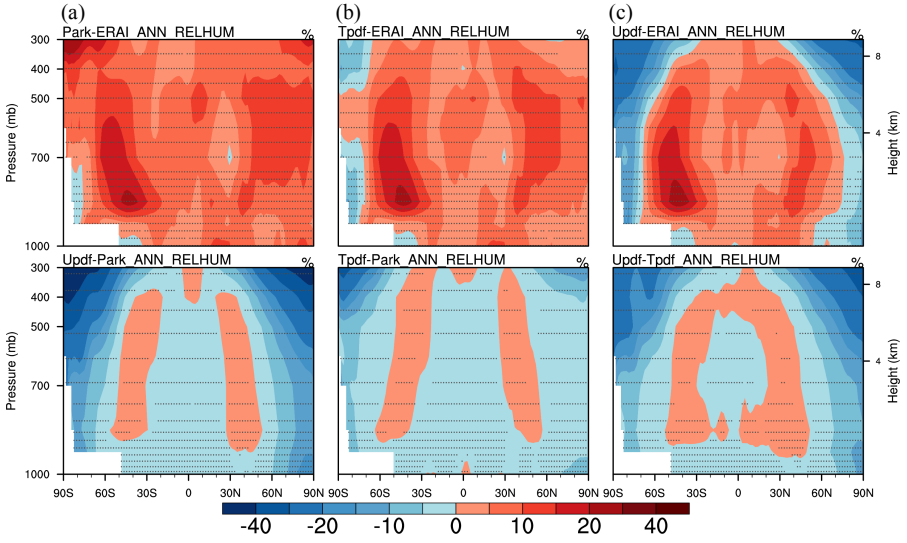

Figure 12. Upper row: latitude–pressure cross-sections of differences in relative humidity (RH) between the simulations and ERA-Interim from (a) Park, (b) T_pdf, and (c) U_pdf schemes. Lower row: differences in RH in pair-wise comparisons of the three cloud macrophysical schemes.

https://doi.org/10.5194/gmd-2020-144
Preprint. Discussion started: 7 July 2020

Geoscientific Model Development
Discussions
Open Access
EGU

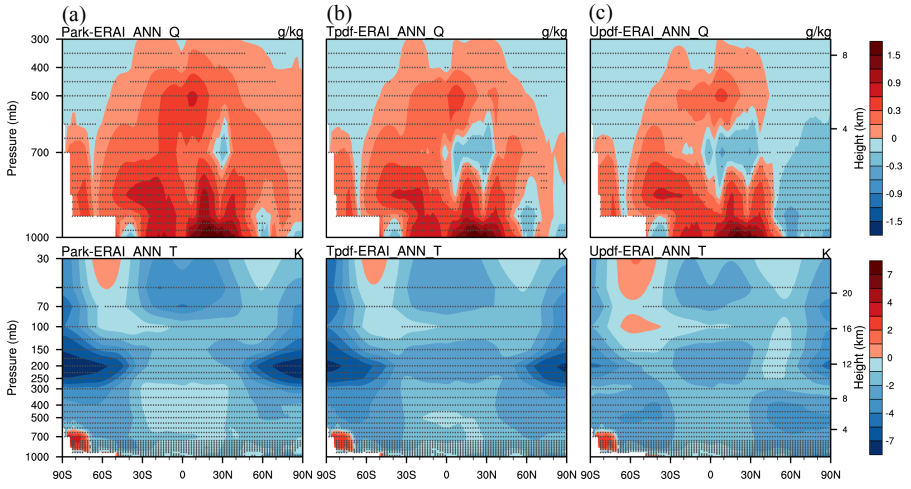

Figure 13. Differences in specific humidity (upper row) and air temperature (lower row) between the simulations and ERA-Interim from the (a) Park, (b) T_pdf, and (c) U_pdf schemes.

https://doi.org/10.5194/gmd-2020-144
Preprint. Discussion started: 7 July 2020

Geoscientific Model Development
Discussions
Open Access
EGU

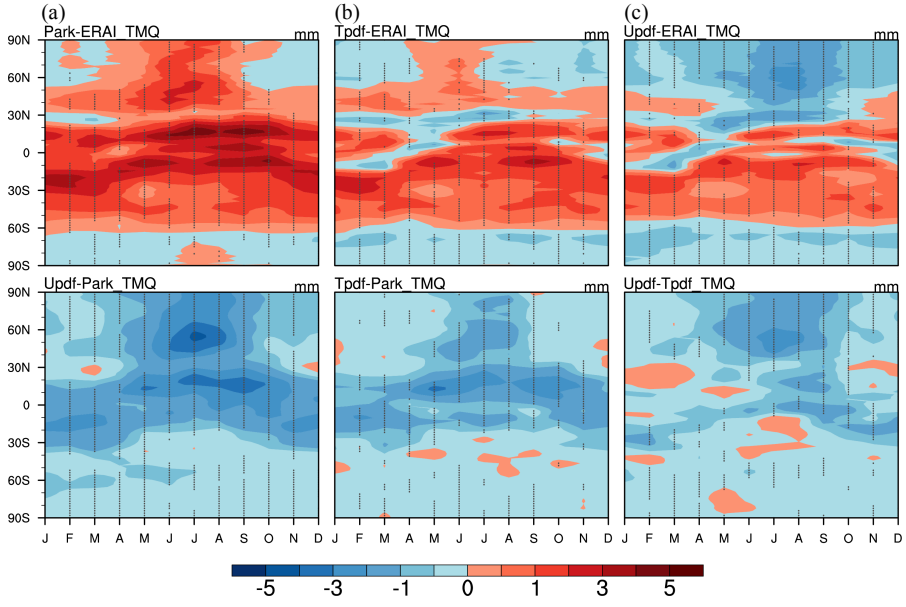

Figure 14. Upper row: differences in annual cycles of zonal mean total precipitable water between the three macrophysical schemes and the ERA-Interim data from the (a) Park, (b) T_pdf, and (c) U_pdf schemes. Lower row: differences in annual cycles of total precipitable water in pair-wise comparisons of the three cloud macrophysical schemes.

https://doi.org/10.5194/gmd-2020-144
Preprint. Discussion started: 7 July 2020

Geoscientific Model Development
Discussions
Open Access
EGU

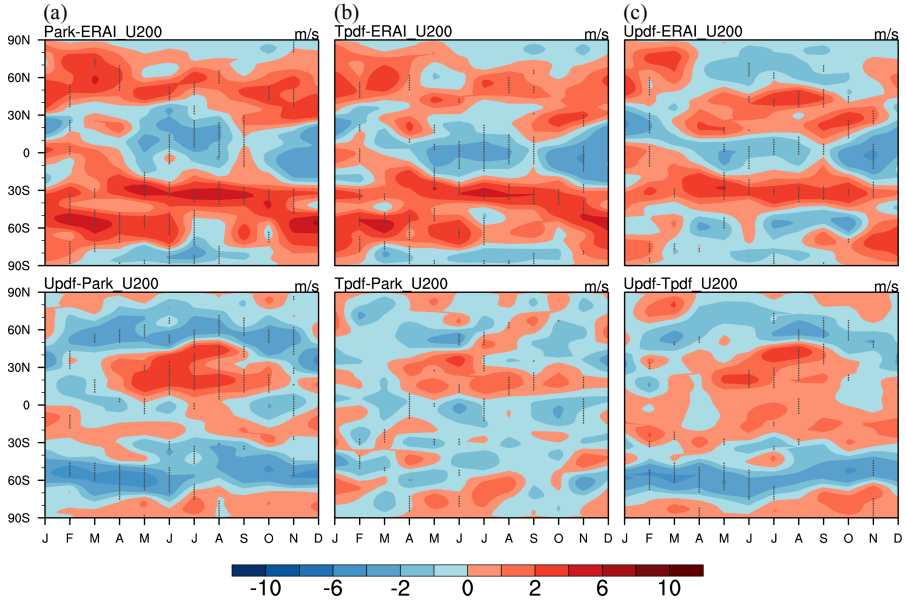

Figure 15. Upper row: differences in annual cycles of zonal wind at 200 mb between the three macrophysical schemes and the ERA-Interim data from the (a) Park, (b) T_pdf, and (c) U_pdf schemes. Lower row: differences in annual cycles of zonal wind at 200 mb in pair-wise comparisons of the three cloud macrophysical schemes.

https://doi.org/10.5194/gmd-2020-144
Preprint. Discussion started: 7 July 2020

Geoscientific Model Development
Discussions
Open Access
EGU

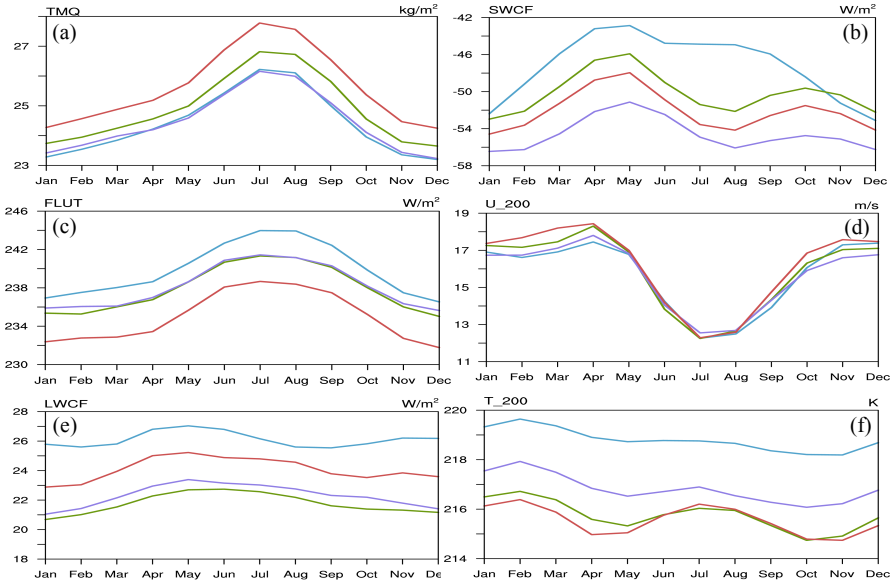

Figure 16. Global annual cycles of (a) total precipitable water, (b) shortwave cloud forcing, (c) net longwave flux at the top of the model, (d) zonal wind at 200 mb, (e) longwave cloud forcing, and (f) air temperature at 200 mb. Colored lines represent observational data (blue) and simulations by the Park (red), U_pdf (purple), and T_pdf (green) schemes.

https://doi.org/10.5194/gmd-2020-144
Preprint. Discussion started: 7 July 2020

Geoscientific Model Development
Discussions
Open Access
EGU

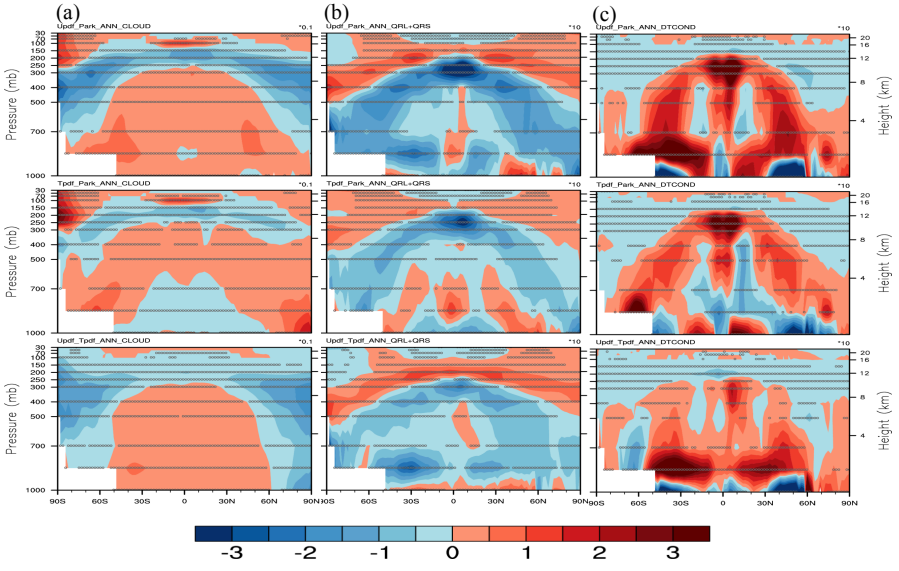

Figure 17. Differences in (a) CF, (b) sum of longwave and shortwave heating rates (QRL+QRS), and (c) temperature trends due to moist processes in the NCAR CESM model (DTCOND) in pair-wise comparisons of the three cloud macrophysical schemes. Upper row: U_pdf and Park; middle row: T_pdf and Park; lower row: U_pdf and T_pdf. A statistically significant difference with a confidence level of 95% is represented in the panels by an open circle using Student's t-test.

https://doi.org/10.5194/gmd-2020-144
Preprint. Discussion started: 7 July 2020

Geoscientific Model Development Discussions
Open Access
EGU

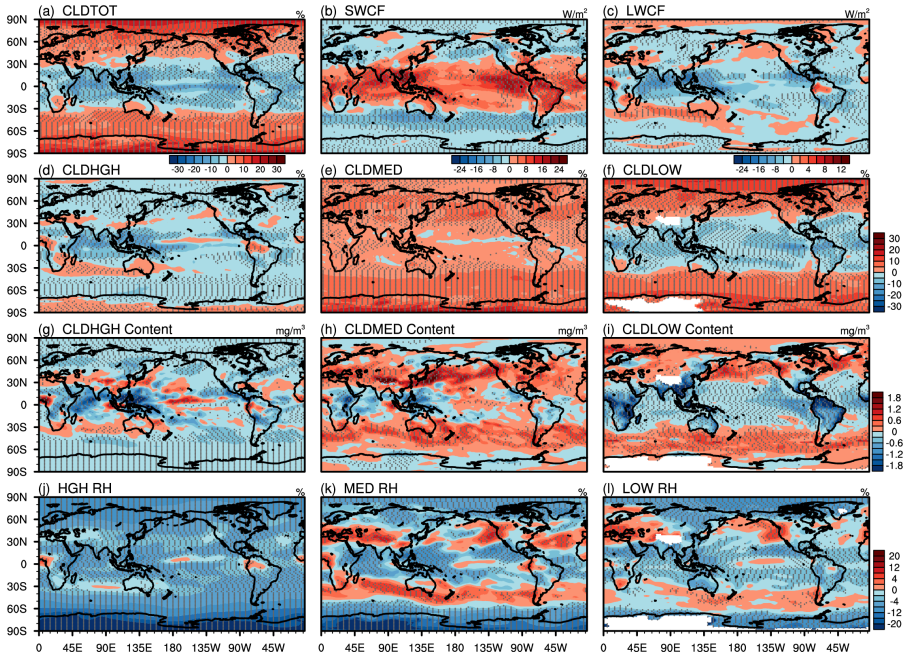

Figure 18. Differences in (a) total cloud fraction, (b) short-wave cloud radiative forcing, (c) long-wave cloud radiative forcing, and cloud fraction of (d) high clouds, (e) middle clouds, and (f) low clouds between the T_pdf and default Park schemes. (g–i) As for (d-f) but for total cloud water content at the three cloud levels. (j–l) As for (g–i) except for averaged RH at the three cloud levels.